HHS Public Access

Author manuscript

Nat Struct Mol Biol. Author manuscript; available in PMC 2023 February 21.

Published in final edited form as:

Nat Struct Mol Biol. 2022 August ; 29(8): 801–812. doi:10.1038/s41594-022-00812-9.

The structure-specific endonuclease complex SLX4/XPF regulates Tus/*Ter*-induced homologous recombination

Rajula Elango[1], **Arvind Panday**[1], **Francis P. Lach**[2], **Nicholas A. Willis**[1], **Kaitlin Nicholson**[1], **Erin E. Duffey**[1], **Agata Smogorzewska**[2], **Ralph Scully**[1,3]

[1]Department of Medicine, Division of Hematology-Oncology and Cancer Research Institute, Beth Israel Deaconess Medical Center and Harvard Medical School, Boston, MA 02215, USA.

[2]Laboratory of Genome Maintenance, The Rockefeller University, New York, NY 10065, USA.

Abstract

Vertebrate replication forks arrested at interstrand DNA crosslinks (ICLs) engage the Fanconi anemia (FA) pathway to incise arrested forks, 'unhooking' the ICL and forming a double strand break (DSB) that is repaired by homologous recombination (HR). The *FANCP* product, SLX4, in complex with the FANCQ/XPF/ERCC4-ERCC1 endonuclease, mediates ICL unhooking. Whether this mechanism operates at replication fork barriers other than ICLs is unknown. Here, we study the role of mouse SLX4 in HR triggered by a site-specific, chromosomal DNA-protein replication fork barrier formed by the *Escherichia coli*-derived Tus/*Ter* complex. We show that SLX4-XPF is required for Tus/*Ter*-induced HR but not for error-free HR induced by a replication-independent DSB. We additionally uncover a role for SLX4-XPF in DSB-induced 'long tract' gene conversion, an error-prone HR pathway related to break-induced replication. Notably, *Slx4* and *Xpf* mutants that are defective for Tus/*Ter*-induced HR are hypersensitive to ICLs and also to the DNA-protein crosslinking agents 5-aza-2'-deoxycytidine and zebularine. Collectively, these findings show that SLX4-XPF can process DNA-protein fork barriers for HR and that the Tus/*Ter* system recapitulates this process.

[3]Correspondence: rscully@bidmc.harvard.edu.

Author Contributions

R.E., A.P., F.P.L., K.N., N.A.W., D.N. and E.E.D. conducted the experiments; R.E., A.S. and R.S. designed the experiments. R.E. and R.S wrote the manuscript.

Declaration of Interests

The authors declare no competing interests.

Peer review Information:

Nature Structural and Molecular Biology thanks Katharina Schlacher and the other, anonymous, reviewer(s) for their contribution to the peer review of this work.

Editor summary:

Elango et al. identify a new class of substrates on which the Fanconi anemia (FA) SLX4-XPF nuclease operates. It mediates homologous recombination at a DNA-protein replication fork barrier and promotes cellular tolerance of DNA-protein crosslinks.

Editor recognition statement:

Primary Handling Editor: Beth Moorefield and Carolina Perdigoto, in collaboration with the Nature Structural & Molecular Biology team.

Keywords

Fanconi anemia; homologous recombination; SLX4; XPF; replication fork stalling; Tus/*Ter*; DSB repair; long tract gene conversion; break-induced replication

Introduction

Chromosomal DNA replication is frequently challenged by events that impede progression of the replication fork. Fork-stalling lesions include various types of DNA damage, unusual DNA secondary structures in undamaged DNA, DNA-protein complexes and products of transcription [1–4]. Interstrand crosslinks (ICLs) are formidable fork barriers, since they covalently link the two parental strands, preventing passage of the replicative helicase. Unless the ICL can be disrupted or bypassed, it is an absolute block to replication fork progression [5–8]. In higher eukaryotes, ICL-stalled forks are repaired by the Fanconi anemia (FA) pathway [9–11]. Cells from FA patients are hypersensitive to ICL-inducing agents, including aldehydes, which are an endogenous source of both ICLs and DNA-protein crosslinks [6,12–15]. FA mutant cells reveal elevated frequencies of ICL-induced 'chromatid-type' aberrations, reflecting a defect in replication-coupled ICL repair. To date, 22 FA genes have been identified.

The fundamental steps of the FA pathway have been revealed by *in vitro* studies of ICL-containing plasmids replicating in frog egg extracts [9,16]. Provided the ICL is not bypassed [7,8], bidirectional fork stalling at the ICL triggers replisome disassembly ('fork collapse'), orchestrated by the E3 ubiquitin ligase TRAIP [17]. Association of the DNA translocase and scaffolding protein FANCM with the stalled fork helps to recruit the FA core complex, a multi-subunit E3 ubiquitin ligase that monoubiquitinates and activates the FANCD2-FANCI heterodimer [9,18–20]. Monoubiquitinated FANCD2-I is a sliding clamp that encircles dsDNA at the stall site [21,22]; in parallel, asymmetric fork reversal may occur [23]. These steps are required for recruitment of the endonuclease scaffold SLX4/FANCP and the associated endonuclease XPF (xeroderma pigmentosum group F)/FANCQ in complex with ERCC1 (excision repair cross complementation group 1) [24–27]. XPF introduces incisions either side of the ICL on one sister chromatid, generating a two-ended double strand break (DSB) opposite an 'unhooked' ICL on the unbroken sister chromatid [25,28–30]. The single stranded (ss)DNA gap opposite the unhooked ICL is filled by translesion synthesis (TLS) DNA polymerases, and the DSB is repaired by conservative HR. Despite these mechanistic insights, it is unclear whether the full FA mechanism is restricted to ICL repair, or whether FA-mediated incisions can induce HR at other types of fork-stalling lesions, such as DNA-protein complexes [31]. In this regard, a molecularly defined system that recapitulates the FA mechanism *in vivo* on a mammalian chromosome has been lacking.

To study repair triggered by replication fork stalling at a defined chromosomal locus of cycling mammalian cells, we adapted the *Escherichia coli* Tus/*Ter* replication fork barrier (RFB) for use in mammalian cells [32]. An array of six 23 bp *Ter* repeats, when targeted to a specific genomic locus of mouse embryonic stem (mES) cells and bound by the Tus protein, triggers bidirectional fork stalling and HR at the Tus/*Ter* RFB. Tus/*Ter*-induced

fork stalling also triggers formation of ~10 kb tandem duplications (TDs) in *Brca1* mutant cells, recapitulating the TD phenotype of *BRCA1* mutant breast and ovarian cancers [33–35]. Thus, although an artificial site-specific DNA-protein fork barrier, the Tus/*Ter* RFB models the impact of certain endogenous fork-stalling lesions—presumably endogenous DNA-protein barriers—on DNA repair and genomic instability. Conservative HR at Tus/*Ter*, also called 'short tract' gene conversion (STGC), is a non-crossover pathway mediated by early components of the FA pathway and the canonical BRCA-Rad51 HR pathway [32,33,36,37]. In contrast, Tus/*Ter*-induced 'long tract' gene conversion (LTGC)—a replicative outcome related to break-induced replication (BIR)—is independent of *BRCA* genes, Rad51 and the FA pathway [32]. Notably, HR induced at a site-specific DNA-protein fork barrier in *Schizosaccharomyces pombe* does not proceed *via* a DSB intermediate [38]. Thus, it is important to determine whether Tus/*Ter*-induced STGC entails an incision step with formation of a DSB intermediate and, if so, how the incision at Tus/*Ter* is controlled. To address these questions, we have studied the role of SLX4 in Tus/*Ter*-induced HR.

SLX4/FANCP encodes a scaffolding protein that binds multiple endonuclease complexes in a cell cycle-dependent manner to cleave branched DNA structures [39–45]. In S phase cells, SLX4 interacts with XPF–ERCC1 *via* the SLX4 MLR (MEI9- Interaction-Like Region) domain, with SLX1 (synthetic lethal of unknown function 1) *via* the SBD (SLX1-binding) domains; and with MutSβ *via* the SLX4 N-terminus [46]. In mitosis, SLX4 additionally binds the MUS81 (methyl methanesulfonate and UV sensitive 81)–EME1 (essential meiotic endonuclease 1) nuclease *via* the SAP (SAF-A/B, Acinus and PIAS) domain. These interactions enable the SLX4 'trinuclease' complex to act on a variety of branched DNA substrates in mitosis, cleaving stalled replication forks at sites of incomplete DNA synthesis and resolving post-replicative Holliday junctions [39–43]. SLX4 contains at its N-terminus two conserved Ubiquitin Binding Domain 4 (UBZ) motifs that facilitate its localization to laser-induced damage sites, potentially implicating these motifs in a similar recruitment mechanism at stalled forks [47–49]. Notably, all clinically-described FA-associated *SLX4/FANCP* mutations described to date are hypomorphic alleles, encoding polypeptides with disrupted UBZ motifs [47,50]. More severe *SLX4* mutations may be incompatible with development [51,52].

In this study, we use CRISPR/Cas9 genome editing to engineer precise, defined mutations in the *Slx4* gene of mouse embryonic stem (mES) cells that carry a reporter of stalled fork- and DSB-induced HR. We systematically examine the role of individual nuclease-interacting domains of SLX4 in stalled fork HR. Our results identify a unique role for the SLX4-XPF complex in Tus/*Ter*-induced STGC and reveal a role for the SLX4-XPF in preserving cell viability in response to chemicals that specifically induce DPCs. We define a requirement for the SLX4 UBZ motifs in the recruitment of SLX4 to stalled forks, providing important insight into the mechanisms that connect clinically-described *SLX4/FANCP* mutations to genomic instability. We also identify an unexpected role for SLX4 in supporting LTGC in the repair of a replication-independent DSB.

Results

Slx4 regulates HR at Tus/*Ter*-stalled replication forks

To study the role of *Slx4* in mammalian stalled fork repair, we used dual CRISPR/Cas9-mediated incisions to introduce defined deletions within the endogenous *Slx4* gene of mES cells that contain a single copy of a 6x *Ter*-HR reporter targeted to the *Rosa26* locus on chromosome VI [32]. In this reporter, HR can be triggered by either Tus/*Ter*-induced fork stalling or by a site-specific DSB induced by the rare-cutting homing endonuclease I-SceI (Fig. 1a). The reporter enables simultaneous flow cytometric quantitation of error-free HR as short tract gene conversion (STGC; GFP^+RFP^-), and aberrant replicative HR responses as long tract gene conversion (LTGC; GFP^+RFP^+). We engineered a 125 bp frame-shift deletion in exon 2 ($Slx4^{\Delta 125}$), thereby disrupting *Slx4* early in the ORF (Fig. 1b). CRISPR/Cas9 targeting frequently generates a non-synonymous deletion within the second allele of the target gene [37,53]. In recognition of this fact, we term the second allele in $Slx4^{\Delta 125}$ clones "$Slx4^{\Delta}$". We assayed two independent *Slx4* mutant clones ($Slx4^{\Delta 125/\Delta}$ #40, 42) and two isogenic clones that received the same CRISPR/Cas9 treatment but retained wild type *Slx4* ($Slx4^{+/+}$ #3, 13) (Fig. 1b). Both $Slx4^{\Delta 125/\Delta}$ clones expressed normal levels of *Slx4* mRNA (Extended data Fig. 1a), suggesting that $Slx4^{\Delta 125}$ may not be a null allele. Colony formation assays showed that $Slx4^{\Delta 125/\Delta}$ mutants are hypersensitive to the ICL-inducing agent mitomycin C (MMC; Fig. 1c).

To measure the impact of *Slx4* disruption on stalled fork HR and DSB-induced HR, we transfected $Slx4^{\Delta 125/\Delta}$ *Ter*-HR reporter cells, in parallel, with *Tus* or *I-SceI* expression vectors and assayed repair products 72 hours post-transfection (see methods). $Slx4^{\Delta 125/\Delta}$ clones revealed a ~4-fold reduction in Tus/*Ter* induced STGC compared to isogenic wild type clones, whereas Tus/*Ter*-induced LTGC was unaltered (Fig. 1d, 1e and 1f). Hence, HR at Tus/*Ter* was skewed in favor of LTGC (Extended data Fig. 1b). In contrast, I-SceI-induced STGC was unaltered in $Slx4^{\Delta 125/\Delta}$ cells, whereas I-SceI-induced LTGC was reduced (Fig. 1d, 1g and 1h). Consequently, the ratio of I-SceI-induced LTGC:Total HR was reduced in $Slx4^{\Delta 125/\Delta}$ cells (Extended data Fig. 1c). These results suggest that mammalian *Slx4* has distinct roles in stalled fork HR (where it promotes STGC) and in conventional DSB-induced HR (where it mediates LTGC).

To avoid generating non-synonymous *Slx4* allelic deletions in subsequent experiments, we established an *Slx4* haploid reporter cell line (here termed $Slx4^{+/-}$). We used dual CRISPR/Cas9 incisions at exon 2 and exon 15 to delete one copy of the entire 19.3 kb gene (Extended data Fig. 1d, 1e and 1f). We retrieved no $Slx4^{-/-}$ clones from this experiment, despite an expected frequency of $(60/262)^2$ = ~13/262 (Extended data Fig. 1d), suggesting that a true *Slx4* null is lethal in mES cells. We used direct sequencing of breakpoint PCR products to identify the deletion breakpoint in $Slx4^{+/-}$ cells and confirmed that the retained allele is wild type at the sgRNA target sites (Extended data Fig. 1f). *Slx4* expression in the $Slx4^{+/-}$ clone was detected at wild type levels, suggesting that transcription is upregulated in compensation for hemizygosity (Extended data Fig. 1g). $Slx4^{+/-}$ cells revealed no increased sensitivity to MMC or to the PARP inhibitor Olaparib (Extended data Fig. 1h and 1i) and

were phenotypically wild type for stalled fork- and DSB-induced HR (Extended data Fig. 1j).

The SLX4 UBZ domain recruits SLX4 to stalled forks for HR

To study the SLX4 UBZ domain in Tus/*Ter*-induced HR, we used dual CRISPR/Cas9-mediated incisions to delete in-frame the UBZ1- and UBZ2-coding regions in *Slx4*$^{+/-}$ *Ter*-HR reporter cells (Fig. 2a, Extended data Fig. 2a). UBZ-encoding mRNA sequences were undetectable in *Slx4*$^{\Delta UBZ/-}$ cells, whereas sequences downstream (encoding MLR, SAP and SBD domains) were expressed at normal levels (Extended data Fig. 2b). *Slx4*$^{\Delta UBZ/-}$ clones were hypersensitive to MMC (Extended data Fig. 2c), but resistant to Olaparib, Hydroxyurea and Camptothecin (Extended data Fig. 2d, 2g, and 2h; mES cells lacking *Brca1* exon 11 served as positive controls in these colony formation assays). Notably, *Slx4*$^{\Delta UBZ/-}$ cells were hypersensitive to 5-aza-2'deoxycytidine and zebularine—two agents that induce DPCs but not ICLs (Extended data Fig. 2e and 2f) [54,55]. A characteristic feature of FA cells is enhanced S/G2 phase accumulation following exposure to MMC [10]. Untreated *Slx4*$^{\Delta UBZ/-}$ cells revealed cell cycle distribution patterns similar to *Slx4*$^{+/-}$ cells (Fig. 2b). However, in response to titrated doses of MMC, *Slx4*$^{\Delta UBZ/-}$ cells accumulated in G2/M more readily than *Slx4*$^{+/-}$ controls and revealed a corresponding reduction in the S-phase fraction (Fig. 2b).

We analyzed repair functions of six independent *Slx4*$^{\Delta UBZ/-}$ clones and six independent isogenic Cas9/sgRNA-exposed *Slx4*$^{+/-}$ clones. Strikingly, Tus/*Ter*-induced STGC was reduced ~6-fold in *Slx4*$^{\Delta UBZ/-}$ clones in comparison to *Slx4*$^{+/-}$ controls (Fig. 2c). I-SceI induced STGC was reduced to a lesser extent (Fig. 2d). Transient expression of wild type human *SLX4* restored Tus/*Ter*-induced STGC to wild type levels in *Slx4*$^{\Delta UBZ/-}$ clones (#2 and #5), but had no impact on *Slx4*$^{+/-}$ controls (#25 and #44) (Fig. 2e). A UBZ 4C>A mutant that specifically disrupts UBZ domain function[24] failed to complement the STGC defect of *Slx4*$^{\Delta UBZ/-}$ cells, despite equivalent levels of expression (Extended data Fig. 2i and Fig. 2j). In the same experiment, expression of wild type *SLX4* or 4C>A had no statistically significant impact on I-SceI-induced STGC in either *Slx4*$^{\Delta UBZ/-}$ or *Slx4*$^{+/-}$ clones (Fig. 2f). The ability of wild type *SLX4* but not the 4C>A mutant to complement the defect in Tus/*Ter*-induced STGC in *Slx4*$^{\Delta UBZ/-}$ cells indicates a specific requirement for the SLX4 UBZ domain in error-free HR (i.e., STGC) at stalled forks. In contrast, the failure of wild type *SLX4* to complement the modest defect in I-SceI-induced STGC in *Slx4*$^{\Delta UBZ/-}$ cells provides no clear evidence of a role for the SLX4 UBZ domain in this function. Thus, *Slx4*$^{\Delta UBZ}$ is a separation-of-function allele that distinguishes control of STGC at stalled forks from STGC at replication-independent DSBs.

The same experiments revealed different effects on LTGC. Tus/*Ter*-induced LTGC was modestly reduced in the six *Slx4*$^{\Delta UBZ/-}$ clones; hence, the ratio of LTGC:Total HR was elevated, reflecting the severe defect in STGC (Extended data Figs. 3a and 3b). Tus/*Ter*-induced LTGC was unaffected by expression of either wild type *SLX4* or the 4C>A mutant (Extended data Fig. 3c). Thus, there is no clear evidence of a role for the SLX4 UBZ domain in Tus/*Ter*-induced LTGC. In contrast, I-SceI-induced LTGC was reduced >2-fold in the six *Slx4*$^{\Delta UBZ/-}$ clones in comparison to *Slx4*$^{+/-}$ controls (Extended data Fig. 3d); as a result,

the ratio of LTGC:Total HR was reduced ~2-fold, reflecting the specific reduction in I-SceI-induced LTGC (Extended data Fig. 3e). Importantly, the LTGC defect was complemented by wild type *SLX4* but not by the 4C>A mutant (Extended data Fig. 3f). Thus, *Slx4*$^{\Delta UBZ}$ is a separation-of-function allele that distinguishes control of LTGC at replication-independent DSBs from LTGC at stalled forks.

To facilitate detection of the endogenous *Slx4* gene product in mES cells, we targeted the 3'end of the residual *Slx4* allele in *Slx4*$^{+/-}$ and *Slx4*$^{\Delta UBZ/-}$ cells with a dual minimal auxin-inducible and SMASh degron containing an 8x HA epitope tag positioned N-terminal of the SMASh degron cleavage site [37,56–58], to generate *Slx4*$^{deg/-}$ and *Slx4*$^{\Delta UBZdeg/-}$ clones (Fig. 2g). *Slx4*$^{deg/-}$ and *Slx4*$^{\Delta UBZdeg/-}$ clones expressed comparable levels of *Slx4* mRNA (Fig. 2h). We detected non-specific bands in the whole-cell extract (WCE), however, a specific HA-tagged gene products were detectable in the chromatin fraction (Extended data Fig. 2k, Fig. 2i). Therefore, we restricted our western blot analyses to chromatin bound Slx4. Activation of the dual degron triggered partial degradation of endogenous SLX4, confirming the specificity of the anti-HA western blot signal. Unexpectedly, the HA-tagged *Slx4*$^{\Delta UBZdeg}$ gene product was more abundant in the chromatin fraction than the wild type protein (Fig. 2i). We used these tools, in combination with chromatin immunoprecipitation (ChIP), to study SLX4 recruitment to Tus/*Ter*-stalled forks. Strikingly, we noted robust accumulation of wild type SLX4-deg at the Tus/*Ter* RFB, but reduced accumulation of SLX4-ΔUBZdeg (Fig. 2j). Thus, the SLX4 UBZ domain mediates Tus/*Ter*-induced STGC by recruiting SLX4 to the site of fork stalling.

SLX4-MUS81 and SLX1 complexes: no role in Tus/*Ter*-induced HR

To study the SLX4-MUS81 interaction in Tus/*Ter*-induced repair, we used Cas9-dual sgRNA incisions to generate in-frame deletions of *Slx4* exons 11–13, encoding the SAP domain, in *Slx4*$^{+/-}$ *Ter*-HR reporter cells (Fig. 3a and Extended data Fig. 4a). The mRNA sequence encoding the SAP domain was undetectable in *Slx4*$^{\Delta SAP/-}$ cells, whereas expression of other *Slx4* elements was at wild type levels (Extended data Fig. 4b). Degron-HA-targeted *Slx4*$^{\Delta SAP/-}$ cells revealed normal levels of HA-tagged gene products (Extended data Fig. 4c). *Slx4*$^{\Delta SAP/-}$ cells were modestly sensitive to MMC but not to Olaparib, 5-aza-2′-deoxycytidine, zebularine, hydroxyurea and camptothecin (Extended data Fig. 5a, 5b, 5c, 5d, 5e and 5f) in comparison to isogenic *Slx4*$^{+/-}$ cells that had been similarly treated with Cas9/sgRNA. We analyzed stalled fork and DSB repair functions in five independent *Slx4*$^{\Delta SAP/-}$ clones and five isogenic *Slx4*$^{+/-}$ clones and found no impact of SAP domain deletion on any of the repair functions measured (Fig. 3b and 3c; Extended data Fig. 4d and 4e). Thus, the interaction of SLX4 with MUS81 is dispensable for Tus/*Ter*-induced and I-SceI-induced HR.

To study the SLX4-SLX1 interaction in Tus/*Ter* induced repair, we used Cas9-dual sgRNA incisions to generate in-frame deletions of *Slx4* exons 13–15, encoding the SBD domain, in *Slx4*$^{+/-}$ *Ter*-HR reporter cells (Fig. 3d and Extended data Fig. 4f). The mRNA sequence encoding the SBD domain was almost undetectable in the *Slx4*$^{\Delta SBD/-}$ cells, whereas expression of other elements of *Slx4* was at normal levels (Extended data Fig. 4g). Degron-HA-targeted *Slx4*$^{\Delta SBD/-}$ cells revealed normal levels of HA-tagged gene products (Extended

data Fig. 4h). *Slx4*$^{\Delta SBD/-}$ cells were insensitive to MMC, Olaparib, 5-aza-2′-deoxycytidine, zebularine, hydroxyurea and camptothecin (Extended data Fig. 5g, 5h, 5i, 5j, 5k and 5l) in comparison to isogenic *Slx4*$^{+/-}$ cells that had been similarly treated with Cas9/sgRNA. We analyzed stalled fork and DSB repair functions in six independent *Slx4*$^{\Delta SBD/-}$ clones and six isogenic *Slx4*$^{+/-}$ clones and found no impact of SBD domain deletion on any of the repair functions measured (Fig. 3e and 3f; Extended data Fig. 4i and 4j). Thus, the interaction of SLX4 with SLX1 is dispensable for Tus/*Ter*-induced and I-SceI-induced HR.

SLX4-XPF binding is required for Tus/*Ter*-induced STGC

To study the SLX4-XPF interaction in Tus/*Ter* stalled fork repair, we used dual sgRNAs to generate in-frame deletion of the MLR-encoding exons 5 and 6 in *Slx4*$^{+/-}$ Ter-HR reporter cells (Fig. 4a, Extended data Fig. 6a). *Slx4* mRNA transcripts in *Slx4*$^{\Delta MLR/-}$ clones lacked the deleted region but were otherwise detected at normal levels (Extended data Fig. 6b). Degron-HA-targeted *Slx4*$^{\Delta MLR/-}$ cells revealed a modest reduction in the levels of HA-tagged gene products (Extended data Fig. 6c). *Slx4*$^{\Delta MLR/-}$ clones were slow-growing compared to isogenic *Slx4*$^{+/-}$ controls that had been similarly exposed to Cas9/sgRNA but had retained wild type *Slx4*. In untreated cells, the proportion of cells in late S/G2/M was elevated ~2-fold in *Slx4*$^{\Delta MLR/-}$ cells in comparison to *Slx4*$^{+/-}$ cells (Fig. 4b). The S-phase fraction was correspondingly reduced. Similarly, following exposure of cells to titrated doses of MMC, *Slx4*$^{\Delta MLR/-}$ cells revealed more dramatic late S/G2/M accumulation and S phase depletion than *Slx4*$^{+/-}$ controls (Fig. 4b). *Slx4*$^{\Delta MLR/-}$ cells were hypersensitive to MMC, 5-aza-2′-deoxycytidine and zebularine but not to Olaparib, hydroxyurea and camptothecin in comparison to *Slx4*$^{+/-}$ controls (Extended data Fig. 6d, 6e, 6f, 6g, 6h and 6i). The slow growth and late S/G2/M accumulation suggest that *Slx4*$^{\Delta MLR/-}$ cells do not resolve replication stress efficiently. To explore this effect further, we analyzed metaphase spreads from *Slx4*$^{+/-}$, *Slx4*$^{\Delta UBZ/-}$ and *Slx4*$^{\Delta MLR/-}$ cultures that were either untreated or exposed to 20 ng/ml of MMC for 12 hours. Both *Slx4*$^{\Delta UBZ/-}$ and *Slx4*$^{\Delta MLR/-}$ cells revealed elevated levels of breaks and radial chromosomes in comparison to *Slx4*$^{+/-}$ controls, but *Slx4*$^{\Delta MLR/-}$ cells revealed a more severe defect than *Slx4*$^{\Delta UBZ/-}$ cells (Fig. 4c, 4d and 4e). Thus, both *Slx4*$^{\Delta UBZ/-}$ and *Slx4*$^{\Delta MLR/-}$ cells display a classical Fanconi anemia chromosome breakage/aberration phenotype. In a second experiment, we additionally analyzed *Slx4*$^{\Delta SAP/-}$ and *Slx4*$^{\Delta SBD/-}$ cells (Extended data Fig. 6j, 6k and 6l). *Slx4*$^{\Delta SAP/-}$ cells were indistinguishable from *Slx4*$^{+/-}$ cells. *Slx4*$^{\Delta SBD/-}$ cells revealed modestly elevated frequencies of breaks and radials compared to *Slx4*$^{+/-}$ cells.

We analyzed stalled fork- and DSB-induced HR in six independent *Slx4*$^{\Delta MLR/-}$ clones and six independent *Slx4*$^{+/-}$ isogenic clones. Tus/*Ter*-induced STGC was almost undetectable in *Slx4*$^{\Delta MLR/-}$ cells, whereas LTGC was detected at wild type levels (Fig. 5a and Extended data Fig. 7a). I-SceI induced STGC was reduced in *Slx4*$^{\Delta MLR/-}$ clones, while I-SceI induced LTGC was marginally reduced (Fig. 5b and Extended data Fig. 7b). A caveat of these results is the possibility that the slow growth of *Slx4*$^{\Delta MLR/-}$ cells might artifactually alter the measured HR frequencies [59]. To address this concern, we performed complementation experiments in *Slx4*$^{\Delta UBZ/-}$ *Ter*-HR reporter cells, which exhibit no proliferation defect. In addition to testing full-length h*SLX4* expression vectors, we generated ‘mini-*SLX4*’ constructs that encode hSLX4 polypeptides that are truncated C-terminal to the BTB

domain and therefore lack the MUS81-binding SAP or SLX1-binding SBD domains [28]. These mini-*SLX4* constructs included wild type, 4C>A and ΔMLR variants (Fig. 5c). Following transient transfection, h*SLX4* was expressed equivalently from each construct, although the wild type mini-SLX4 protein was more abundant than other products (Fig. 5d and 5e). Expression of mini-*SLX4* complemented the defect in Tus/*Ter*-induced STGC in *Slx4*$^{\Delta UBZ/-}$ cells as efficiently as wild type *SLX4* (Fig. 5f). Importantly, both full length *SLX4*ΔMLR and mini-*SLX4*ΔMLR failed to complement the defect in Tus/*Ter*-induced STGC in *Slx4*$^{\Delta UBZ/-}$ cells, behaving similarly to mini-*SLX4*4C>A. No significant effects of any of these constructs were observed on Tus/*Ter*-induced STGC in *Slx4*$^{+/-}$ cells, and I-SceI-induced STGC was unaffected by any *SLX4* construct in either cell type (Fig. 5f and 5g). These findings show that intact SLX4 UBZ and MLR domains are independently required for Tus/*Ter*-induced STGC. The absence of interallelic complementation between endogenous *Slx4*$^{\Delta UBZ}$ and exogenous *SLX4*ΔMLR alleles suggests that intact UBZ and MLR domains must each be present on the same SLX4 molecule in order for SLX4 to mediate Tus/*Ter*-induced STGC.

In the same experiments, Tus/*Ter*-induced LTGC was unaffected by any of the above-noted h*SLX4* constructs in either *Slx4*$^{\Delta UBZ/-}$ or *Slx4*$^{+/-}$ cells (Extended data Fig. 7c). In contrast, I-SceI-induced LTGC, which is specifically impaired in *Slx4*$^{\Delta UBZ/-}$ cells, was complemented by expression of full-length wild type *SLX4* (consistent with our previous experiments), but not by the ΔMLR mutant (Extended data Fig. 7d). Similarly, wild type mini-*SLX4* complemented the defect in I-SceI-induced LTGC, whereas mini-*SLX4* mutants 4C>A and ΔMLR failed to do so. These results suggest that I-SceI-induced LTGC requires the same elements of SLX4 that are required for Tus/*Ter*-induced STGC.

The XPF nuclease domain in Tus/*Ter*- and I-SceI-induced STGC

The above findings implicate the SLX4-XPF interaction in Tus/*Ter*-induced STGC. We therefore established tools to study XPF in stalled fork repair. We used CRISPR/Cas9 with dual sgRNA targeting to delete one entire ~42.3 kb *Xpf* allele in *Ter*-HR reporter cells (Extended data Fig. 8a and 8b). *Xpf* expression was reduced by ~50% in *Xpf*$^{+/-}$ cells compared to an isogenic *Xpf*$^{+/+}$ clone, implying an absence of transcriptional compensation for hemizygosity (Extended data Fig. 8c). Nonetheless, *Xpf*$^{+/-}$ *Ter*-HR reporter cells revealed wild type levels of the XPF binding partner ERCC1, MMC and Olaparib resistance, and repair frequencies (Extended data Fig. 8d, 8e, 8f and 8g). (We were unable to detect the endogenous XPF protein in mES cells.) To determine whether the XPF nuclease domain contributes to stalled fork HR, we used Cas9 with dual sgRNAs to delete in-frame the nuclease domain-encoding region of *Xpf* in *Xpf*$^{+/-}$ cells (Fig. 6a and 6b). We obtained one *Xpf*$^{Nuc/-}$ clone containing an in-frame deletion (#1) and three that contained a frameshift (#2, #11, #13). Analysis of *Xpf* expression in each mutant clone revealed the absence of nuclease domain-encoding sequences but normal levels of expression of regions encoding the upstream helicase domain and the downstream HhH2 domain (Extended data Fig. 8h). Western blot analysis of the HhH2-binding XPF partner ERCC1 in whole cell extracts revealed variably reduced abundance of ERCC1 in *Xpf*$^{Nuc/-}$clones (Extended data Fig. 8i). Chromatin association of ERCC1 was detected in *Xpf*$^{Nuc/-}$clone #1 but not in the three *Xpf*$^{Nuc/-}$ frameshift clones, suggesting that interaction of XPF with ERCC1 is required for

chromatin association of ERCC1 (Extended data Fig. 8j). All four *Xpf*$^{Nuc/-}$ clones displayed a proliferative defect similar to that of *Slx4*$^{\Delta MLR/-}$ cells, associated with in an increase in the G2/M fraction and a reduction in the S-phase fraction in unperturbed cells (Extended data Fig. 8k). Similarly, following exposure of cells to titrated doses of MMC, *Xpf*$^{Nuc/-}$ cells revealed more dramatic G2/M arrest and S phase depletion than *Xpf*$^{+/-}$ controls. *Xpf*$^{Nuc/-}$ cells were hypersensitive to MMC, 5-aza-2'deoxycytidine and zebularine, and modestly sensitive to Olaparib and camptothecin, in comparison to *Xpf*$^{+/-}$ controls (Fig. 6c, 6d, 6e, 6f and 6h). *Xpf*$^{Nuc/-}$ cells were resistant to hydroxyurea treatment (Fig. 6g). We prepared metaphase spreads from *Xpf*$^{Nuc/-}$ or *Xpf*$^{+/-}$ cells that were either untreated or exposed to 20 ng/ml MMC. *Xpf*$^{Nuc/-}$ cells revealed dramatically elevated frequencies of MMC-induced chromatid breaks and radials, consistent with the status of *XPF/FANCQ* as a FA gene (Fig. 6i, 6j and 6k).

We analyzed stalled fork and DSB repair functions in each of the four *Xpf*$^{Nuc/-}$ *Ter*-HR reporter clones and four isogenic *Xpf*$^{+/-}$ clones. Similar to *Slx4*$^{\Delta MLR/-}$ cells, *Xpf*$^{Nuc/-}$ cells revealed near-complete loss of Tus/*Ter*-induced STGC (Fig. 6l) but no alteration in Tus/*Ter* induced LTGC (Extended data Fig. 8l). We also noted a significant reduction in I-SceI induced STGC (Fig. 6m) and a modest reduction in I-SceI induced LTGC (Extended data Fig. 8m). Thus, *Xpf*$^{Nuc/-}$ cells phenocopy *Slx4*$^{\Delta MLR/-}$ cells in stalled fork repair. The slow growth phenotype of *Xpf*$^{Nuc/-}$ cells suggests that these repair frequencies should be interpreted with caution. However, all of our experiments point to SLX4-XPF as a critical and specific mediator of Tus/*Ter*-induced STGC. Further, the *Slx4* and *Xpf* mutants with the most severe FA phenotype exhibited the most profound impairment of Tus/*Ter*-induced STGC and were hypersensitive to DPC-inducing agents.

Discussion

We show here that the structure-specific endonuclease scaffold SLX4 has a critical and specific function in conservative HR (i.e., STGC) at Tus/*Ter*-stalled forks. SLX4 ubiquitin-binding UBZ and XPF-binding MLR domains are required for Tus/*Ter*-induced STGC, while the SAP and SBD domains are dispensable, excluding a requirement for the mitosis-associated SLX4 trinuclease complex. Taken together, our findings suggest that a major function of SLX4 in Tus/*Ter*-induced STGC is to position XPF at the stalled fork, promoting XPF-mediated incision of the bidirectionally Tus/*Ter*-arrested fork (Fig. 7). Such a function would recapitulate the critical role of SLX4-XPF in the 'unhooking' step of ICL repair [9,25,30], with the exception that only one XPF-mediated incision would be required to generate a two-ended DSB at Tus/*Ter* because of the absence of a crosslink. This model explains why SLX4 plays a major role in Tus/*Ter*-induced STGC but not in I-SceI-induced STGC. In the former case, if SLX4-XPF coordination at the stalled fork were defective, production of a DSB at the stall site would be suppressed, resulting in low levels of HR. In the latter case, the DSB is induced by the I-SceI endonuclease, bypassing any requirement for SLX4-XPF in DSB formation. SLX4-XPF might have additional generic roles in HR, such as in flap-processing.

Key components of the FA pathway required for efficient Tus/*Ter*-induced STGC include FANCM [37], the FA core complex [33,37], the BRCA-Rad51 pathway [60] and SLX4-XPF (this

study). In light of these findings, it will be important in future to determine whether Tus/*Ter*-induced STGC requires TRAIP-mediated CMG ubiquitination [17], monoubiquitination of FANCD2-FANCI [25] and/or a fork reversal step [23]. If, indeed, the full FA mechanism is required for Tus/*Ter*-induced STGC, this would extend the scope of the FA pathway beyond ICL repair and indicate that the FA pathway can also process some DNA-protein replication fork barriers for HR [31]. In support of this idea, we find that cells defective for SLX4-XPF are hypersensitive to 5-aza-2'-deoxycytidine and zebularine. These cytidine analogs are incorporated into DNA and trap de novo DNA methyltransferases (DNMTs) in chromatin as covalent complexes (i.e., DPCs), but do not form ICLs [54,55]. Importantly, the cellular toxicity of 5-aza-2'-deoxycytidine is caused by its capacity to cross-link DNMTs to DNA, not by downstream effects on DNA methylation [54]. Although it has been shown that the FA pathway is not necessary for repair of one class of DPCs, some DPCs encountered during replication might escape proteolytic mechanisms of DPC bypass and be processed by the FA pathway for HR [31,61–64]. Ongoing experiments are underway to determine whether FA pathway components in addition to SLX4 and XPF are involved in 5-aza-2'-deoxycytidine resistance. In this regard, aldehydes, a class of chemicals to which FA mutant cells are hypersensitive, are known to form both ICLs and DPCs [6,12–15]. The Tus/*Ter* system may prove to be a useful model of FA-mediated repair of endogenous DPCs.

We show that a key function of the SLX4 UBZ domain is to support efficient retention of SLX4 at the stall site. As noted above, specific inactivation of UBZ domain function is a common defect of clinically-described *FANCP* mutations [47,50]. Our data suggest that a key defect in *FANCP* mutant FA patient cells is reduced retention of SLX4 at stalled forks. Unlike the true *SLX4* null, which may be cell lethal when homozygous [51,52] (and this study), germ line homozygous *SLX4* ΔUBZ mutations may be compatible with human development because the mutation is hypomorphic—reducing, but not abolishing, SLX4 action at stalled forks.

Unexpectedly, we identified SLX4 as a mediator of DSB-induced LTGC. This finding might appear to connect DSB-induced LTGC to mitotic DNA synthesis (MiDAS), which is mediated by SLX4 [65], MUS81 [66] and SLX1 [67]. However, interaction of SLX4 with MUS81 or SLX1 is dispensable for DSB-induced LTGC, i.e., there is no indication of a role for the mitotic SLX4 trinuclease complex. Instead, DSB-induced LTGC requires the SLX4 UBZ and MLR domains, implicating ubiquitin chain binding and XPF in the mechanism. Further studies will be needed to decipher how SLX4-XPF-mediated incisions contribute specifically to DSB-induced LTGC.

Methods

Molecular biology and sgRNA oligos

The 6x*Ter*-HR reporters used were assembled using standard cloning methods described previously for the 6x*Ter*-HR reporter [32,33]. Derivation of Tus and I-SceI expression plasmid are described in [32,68]. *Ter*-containing plasmids were amplified in JJC33 (Tus^-) strains of *E. coli*. All plasmids used for transfection were prepared by endotoxin-free maxiprep (QIAGEN Sciences). All primers used for genotyping, RT-qPCR, sgRNA synthesis, and chromatin immunoprecipitation were purchased from Life Technologies.

Generation of mouse *Slx4* and *Xpf* mutant cell lines and cell culture

Slx4 mutant cell lines were derived from a conditional mouse *Brca1*$^{fl/exon11}$ *Ter*-HR reporter ES cell line [32]. This founder cell line contains a single copy of the 6x *Ter*-HR reporter cassette, targeted to the *Rosa26* locus and verified by southern blot. Mouse ES cells are routinely thawed onto plates coated with mouse embryonic fibroblast (MEF) feeders, maintained in ES medium on gelatinized plates, and regularly tested for mycoplasma infection by Myco-Alert assay (Lonza). *Slx4* mutant cell lines were generated using CRISPR/Cas9 mediated mutation of the *Slx4* locus. The genotype of each cell line was defined directly using specific PCR testing and cell lines were re-genotyped on multiple occasions. sgRNAs targeting Cas9 to the *Slx4* locus were transcribed *in vitro* using the Engen sgRNA Synthesis kit (New England Biolabs E3322S), purified using the RNA Clean and Concentrator Kit (Zymo Research, R1017), and verified by denaturing 10% TBE-urea PAGE. Cas9-sgRNA RNP was pre-assembled *in vitro* in OptiMEM by mixing Spy NLS Cas9 (New England Biolabs, M0646T) and purified sgRNA. Cells were co-transfected with either 0.45 μg Cas9(1.1) expression plasmid and 0.05 μg of each purified sgRNA using Lipofectamine 2000 (Invitrogen). After 72 hr, transfected cells were plated onto 6-cm dishes containing feeder MEFs without selection. Individual clones were picked for expansion between 9 and 14 days later and *Slx4* mutant clones were identified by PCR and confirmed by sequencing. *Slx4* targeting sgRNA sequences including PAM: *Slx4*$^{\Delta 125/\Delta}$ 5’ exon 2 (5’ CCT TCC TGT TTC ACG ACA ACT GG 3’), *Slx4*$^{\Delta 125/\Delta}$ 3’ exon 2 (5’ ATC CCC CCA AAA GAC TGC ACT GG 3’), *Slx4* hemizygote exon 2 (5’ ATC CCC CCA AAA GAC TGC ACT GG 3’), *Slx4* hemizygote exon 15 (5’ ATC CTT TTT CTT TCG GC CTG AGG 3’); *Slx4 ΔUBZ 5’* (5’ ATG ACA GCC TGG AGG AGA AGG GG 3’), *Slx4 ΔUBZ 3’* (5’ ACA GCC TGA AGC AGG AGT TGG GG 3’); *Slx4 ΔMLR 5’* (5’ CCA AAA GGG AGC CAA GGA GGA GG 3’), *Slx4 ΔMLR 3’* (5’ GGG CAT TGG GAC ACA ATT GGA GG 3’); *Slx4 ΔSAP 5’* (5’ CCA GAA CTC GGA AGC CAG ACA GG 3’), *Slx4 ΔSAP 3’* (5’ GGT AGT TCT GCG GGT ATC TGG GG 3’); *Slx4 ΔSBD 5’* (5’ CGC AGA ACT ACC TTG TCG CCA GG 3’), *Slx4 ΔSBD 3’* (5’ GAA AAA GGA TCA GAA ATG ACA GG 3’); sgRNA targeting Slx4 dual degron (5’ ATC CTT TTT CTT TCG GCC TGA GG 3’); *Xpf* hemizygote 5’ UTR (5’ GTG CGG CCG CGG TCC GAA GGG 3’), *Xpf* hemizygote exon 11 (5’ CAA ACA GCT CGG CTG TGG CGT GG 3’); *Xpf*$^{Nuc/-}$ 5’ (5’ CTC TGC CTT CCC GTT CTT CGG GG 3’), *Xpf*$^{Nuc/-}$ 3’ (5’ ACC AGA GCA GCC GCA AAC GCG GG 3’).

Recombination assays

These assays were performed as described in detail in [69].Briefly, 1.6×10^5 cells were co-transfected in suspension with 0.5 mg empty vector, pcDNA3b-myc NLS-Tus, or pcDNA3b-myc NLS-I-SceI using Lipofectamine 2000 (Invitrogen). GFP+RFP–, GFP+RFP+ and GFP–RFP+ frequencies were scored 72 hours after transfection by flow cytometry Beckman Coulter CytoFlex LX. For each duplicate sample condition, $3–6 \times 10^5$ total events were scored. Repair frequencies presented are corrected for background events and for transfection efficiency (50–85%). Transfection efficiency was measured by parallel transfection with 0.05 mg wild type GFP expression vector and 0.45 mg empty vector. For transient hSLX4 rescue experiments, 1.6×10^5 cells were co-transfected in suspension with 0.4 mg empty vector, pcDNA3b-myc NLS-Tus [32], or pcDNA3b-myc NLS-I-SceI [68],

and either 0.1 mg empty vector and pHIV- 3xFLAG-AttB1-hSlx4-AttB2- NatR-T2A-hCD52 and all other Slx4 domain mutant derivatives using Lipofectamine 2000.

Colony formation assay

Approximately 2000 ES cells were plated on 6 cm tissue culture dishes coated with 0.2% gelatin. 18–20 hours after plating, MMC, Olaparib, 5-aza-2′-deoxycytidine or Zebularine was added to the media. After 7–10 days, cells were fixed using Carnoy's fixative (75% methanol + 25% glacial acetic acid) and stained with crystal violet. Colonies were counted using a Celigo machine. Graphs represent the mean of duplicate samples from three independent experiments. The experiments were blinded during colony counting. Note: all colony formation assays were performed as a single experiment, with subsets of treatment groups shown in individual figures. *Brca1* exon 11 mutant mES cells served as positive controls for sensitivity to MMC and olaparib. This control is shown in **Supplementary Fig. 2c**-**2f**.

RT-qPCR

RNA extraction was performed using QIAGEN RNeasy Mini Kit (QIAGEN Sciences,). All analyses of *Gapdh* and genes of interest were performed using an Applied Biosystems 7300 Real time PCR System using Power SYBR Green RNA-to CT ™ 1-Step Kit (Applied Biosystems, Foster City, CA).Primers for RT-PCR: *Gapdh* sense (5' CGT CCC GTA GAC AAA ATG GT 3'); *Gapdh* antisense (5' TCG TTG ATG GCA ACA ATC TC 3'); *Slx4 exon2 frameshift* sense (5' CAG AGA CAC CAA AAG GTG CTA ACC 3); *Slx4 exon2 frameshift* antisense (5' GCA CGG ACT CCA AAC CTG TCC AGT 3'); *Slx4 hemizygote* sense (5' CAG AGA CAC CAA AAG GTG CTA ACC 3'); *Slx4 hemizygote* antisense (5' GCA CGG ACT CCA AAC CTG TCC AGT 3'); *Slx4-UBZ* sense (5' GCA ACA TGT GAA CAG ATG CCT); *Slx4-UBZ* antisense (5' TTG GTG GTG AGG AAC GGT TT 3'); *Slx4-MLR* sense (5' ACC ACC AAA AGG GAG CCA AG 3'); *Slx4-MLR* antisense (5' CTT GCG ACT TTT CTT CTC TGC T 3'); *Slx4-SAP* sense (5' CAG AGA CAC CAA AAG GTG CTA ACC 3'); *Slx4-SAP* antisense (5' GCA CGG ACT CCA AAC CTG TCC AGT 3'); *Slx4-SBD* sense (5' CTG CAA CCC TTC AAG GTT GCC AAC 3'); *Slx4-SBD* antisense (5' GAG GAG CTT TTA GAG CTA AAG GAG 3'), *Xpf hemizygote* sense (5' GGG AAA CCT CTG AGG GTT TAC TTT 3'), *Xpf hemizygote* antisense (5' CTA GCT TTT TCT CTT ATG AGC TTT 3'), *Xpf helicase* sense (5' GTC AGA ATT CAG GTT GGC TTT TCC 3'); *Xpf helicase* antisense-(5' TTG TTT CTT GAA CTT CTG GAC TCG 3'), *Xpf nuclease* sense (5' GAA AAG CTC ATA AGA GAA AAA GCT 3'); *Xpf nuclease* antisense-(5' CTC CTG GCC ACC GGC TTT CCG AGT 3'); *Xpf Hhh2* sense (5' GAA GAT GCC TGG GGT CAA CGC CAA 3'); *Xpf Hhh2* antisense-(5' AGG AAG TCG TGC AGC TGC TTG GCA T 3'). N-terminal FLAG tagged human SLX4 sense (5' ATG TGA ACA GGT GCT TGG ATG AAG 3'), antisense (5' ATC ACT GAA GCT GAA CAT GGG TGG 3'). mRNA levels were measured in technical triplicates. Target gene expression level was normalized to *Gapdh* using the $2^{-\Delta CT}$ method and the mutants were normalized to the corresponding wild-type.

Isolation of Chromatin-bound Slx4 and ERCC1 western blot

~10×10^6 cells were freshly harvested and washed with 1x PBS and lysed in 5 volumes of chilled A1 buffer (50mM HEPES,140mM Nacl,1mMEDTA,10%glycerol,0.5% NP-40,0.25% TritonX-100,1mM DTT, and 1x protease inhibitor). Each lysate was centrifuged at 1,100 x g at 4 °C for 2 min and the supernatant was discarded. Pellets were resuspended by gentle pipetting in A1 buffer and samples were incubated for 10 minutes on ice. Each suspension was centrifuged at 1,100 x g at 4 °C for 2 min and the supernatant again discarded. Pellets were resuspended by gentle pipetting in 2 volumes of ice cold E2 buffer (10mM Tris-HCl pH-8,200mMNacl, 1mM EDTA and 0.5mM EGTA, and 1x Protease inhibitor). Each suspension was centrifuged at 1,100 x g at 4 °C for 2 min and the supernatant discarded. Pellets were resuspended by gentle pipetting with A1 buffer and incubated for 10 minutes on ice. Each suspension was centrifuged at 1,100 x g at 4 °C for 2 min and the supernatant discarded. Pellets were resuspended by gentle pipetting in 2 volumes of ice cold E3 buffer (500mM Tris-HCl pH-6.8, 500mMNacl and 1x Protease inhibitor. Each sample was sonicated in a water bath using Diagenode Bioruptor 300 with attached 4°C chiller cycling 30 sec on and 30 sec off on high setting for 5 min. Sonicated samples were centrifuged at 16,000xg for 15 min at 4°C. The supernatant corresponding to the chromatin fraction was transferred and subjected for western blot analysis using following antibodies; anti-HA (Abcam ab9110, 1:1000), anti-ERCC1 (Santacruz sc-17809, 1:250), Histone H3 (Abcam ab1791, 1:3000).

Chromatin immunoprecipitation Assay

Chromatin immunoprecipitation was performed as described previously [70]. Transfection of 2.0×10^5 *Ter*-HR reporter cells of the genotypes noted was performed with 0.5 μg empty vector, pcDNA3β-MYC NLS-I-SceI or pcDNA3β-MYC NLS-Tus-F140A-3xFlag using Lipofectamine 2000 (Invitrogen). 10 million cells were collected 24 hours after transfection and fixed in 1% formaldehyde supplemented serum free media. Fixation was quenched by addition of glycine to 125 mM. Cells were lysed in lysis buffer (0.1% SDS, 20 mM EDTA, 50 mM Tris pH 8.1) containing protease inhibitor (Roche protease inhibitor, Roche 13539320). Chromatin shearing to ~500 bp was accomplished using Diagenode Bioruptor 300 with attached 4°C chiller for 20 cycles, 15 seconds on and 30 seconds off at medium setting. To avoid non-specific binding to protein A/G beads, 100 μl lysates for each ChIP sample were precleared by the addition of 10 μl activated Magna ChIP magnetic beads (Millipore Sigma, 16–663) in ChIP dilution buffer (1% Triton-X-100, 2mM EDTA, 150mM NaCl, 20mM Tris pH 8.1) and incubation for 1 hr at 4°C with gentle mixing. After removal of beads by magnet, for each immunoprecipitation, 7 μl of anti-HA (Abcam ab9110) was added and mixed for 12 hours at 4°C followed by addition of 10 μl activated Magna ChIP beads and mixing for 16 hours at 4°C. Beads were washed six times in ice-cold ChIP RIPA buffer (50mM HEPES pH 7.6, 1mM EDTA, 7 mg/mL sodium deoxycholate, 1% NP-40) followed by two washes in ice-cold TE (10 mM Tris pH8.0, 1 mM EDTA). Crosslinks were reversed and DNA was eluted by incubation in 100 μL Elution buffer (1% SDS, 200mM sodium bicarbonate, 5.6 μg/mL RNAse A) overnight at 65°C. Protein was removed by proteinase K digest for 30 min at 55°C. Released DNA was purified by Qiagen PCR Purification column (Qiagen, 28106) and analyzed by qPCR on an ABI Prism 7300 or QuantStudio3 using SYBR Green (Applied Biosystems, 4368702). Primers for qPCR:

+109 bp sense (TCC GGA TAG GGA TAA CAG GGT A); +109 bp antisense (GTC GGC CAT GAT ATA GAC GTT G); 128 bp sense (GAG CGC ACC ATC TTC TTC A); 128 bp antisense (TCC CTA CGA TGC CCT TCA). Data are presented as the mean calculated from three independent experiments (n = 3) normalized against untreated controls (empty vector) and control locus (beta-actin) using the $2^{-\Delta\Delta CT}$ method [71].

Cell Cycle Analysis

ES cells were grown on a 6-well plate until ~70% confluent. Cells were treated with varying concentrations of MMC for 12 h and compared with untreated controls. After 12h, cells were pulsed with 10 μM BrdU for 15 min. Harvested cells were then washed with pre-chilled 1x PBS pH 7.0 by gently pipetting it and spun at 1000 rpm for 5 mins. Supernatant was discarded and the pellet was gently resuspended in 50μl PBS. Cells were fixed by adding 5mL of chilled 70% Ethanol in a dropwise manner while gently but constantly vortexing to prevent clumping. Fixed cells are stored at 4°C in the dark. Before immunostaining for BrdU, cells were spun at 1000rpm for 5 mins to remove the ethanol. While gently vortexing, 0.5mL of 2M HCl, 0.5% Triton-X-100 solution was added in a dropwise manner to denature DNA. Cells were incubated at RT for 30 mins, with intermittently vortexing approximately every 10 mins. Excess acid was removed by spinning and cells were neutralized using 1mL 0.1M Sodium Borate Decahydrate. Once the neutralizing solution is removed, resuspend pellet in 50–100μl of 1xPBS containing 1%BSA. BrdU was counterstained using anti-BrdU antibody (Abcam ab8039, 1:100) and cells were incubated at RT for 30 mins in the dark. Cells were then washed with 5mL chilled 1xPBS containing 20mM HEPES pH 7.4, 0.5% tween-20 to remove excess antibody. A secondary FITC-conjugated rabbit anti-mouse antibody (Jackson Immunoresearch, 115–095-146–1:50) was used and cells were incubated at RT for 30 mins in the dark. Cells were then washed with 5mL chilled 1x PBS containing 20mM HEPES pH 7.4, 0.5% tween-20 to remove secondary antibody. Cells were resuspended with 300μl of solution containing 38mM sodium citrate, 69μM propidium iodide, 5μl/mL RNaseA in the dark for 15 mins at 37°C. Approximately 10^4 events were acquired using Cytoflex LX and the results were analyzed using FloJo software.

Chromosomal breakage assay

~ 3×10^6 adherent cells were either untreated or treated with 0.02μg/mL MMC for 12h. Cells were arrested with colcemid (0.17 μg per ml of media) for 20 min. Cells were harvested and incubated at 37°C in 0.075 M KCl for 10 mins and fixed in freshly prepared methanol:glacial acidic acid (3:1 vol/vol). Cells were stored at 4°C at least overnight. Cells were dropped onto wet slides and air dried at 40°C for 60 min before staining with KaryoMAX Giemsa (Invitrogen) Gurr Buffer for 3 min. After rinsing with fresh Gurr Buffer followed by distilled water, the slides were fully dried at 40 °C for 60 min and scanned using the Metasystems Metafer application. The experiments were randomized and breaks, and radial chromosomes were scored by a person blinded to the identity of the samples.

Statistical methods

Data shown represents the arithmetic mean and error bars represent either the standard error of the mean (s.e.m.) or standard deviation (s.d.) of between three (n = 3) and nine (n = 9)

independent experiments (as noted in each Figure Legend). Data points for each independent experiment were typically collected as the mean of technical duplicates. This mean value was taken as the solitary data point for that individual experiment. The arithmetic mean of samples collected for groups of independent experiments for repair frequency statistical analysis, was calculated and data points for each independent experiment used to calculate the mean and s.e.m., calculated as standard deviation/√n, (n indicates the number of independent experiments). Differences between sample pairs repair frequencies and fold enrichment for ChIP were analyzed by Student's two-tailed unpaired *t*-test, assuming unequal variance. One-way ANOVA statistical analysis of greater than three samples was performed when indicated. P-values are indicated in the figure and the P-value code for each figure is as written in the Fig. 1 legend. No statistical methods were used to predetermine sample size. The experiments were not randomized, and investigators were not blinded to allocation during experiments and outcome assessment. All statistics were performed using GraphPad Prism v7.0d software.

Extended Data

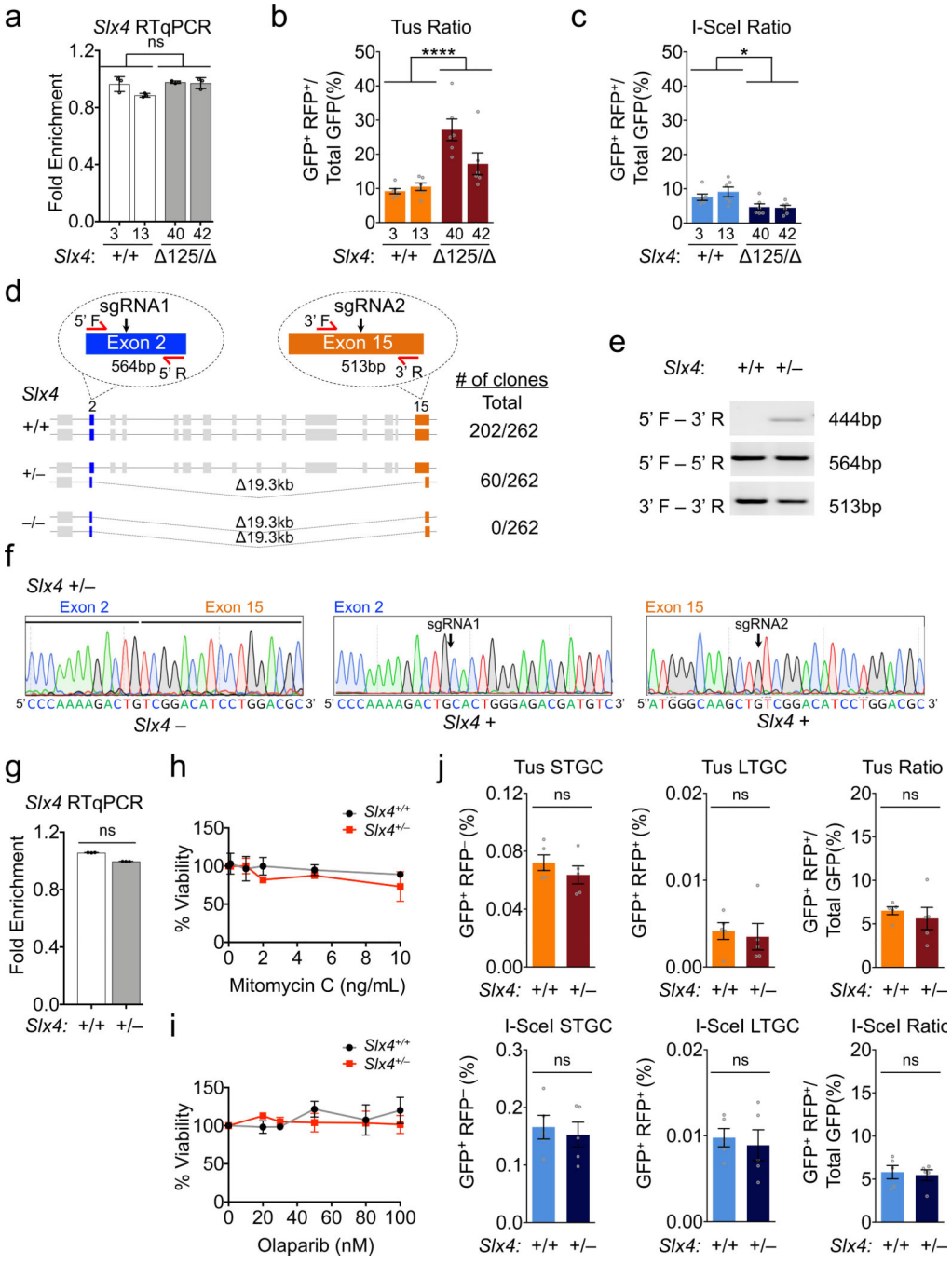

Extended Data Fig. 1. Characterization of *Slx4*$^{\Delta 125/\Delta}$ cells

a. RT-qPCR analysis of *Slx4* mRNA normalized to *Gapdh* mRNA using the $2^{-\Delta CT}$ method in three independent experiments. Each data point is an average of three technical replicates. Data shows mean of three independent biological replicates (n=3), Error bars: standard deviation (s.d.) Statistical analysis using Student's *t*-test. **b** and **c**. Ratio of Tus/Ter-induced (**b**) and I-SceI-induced (**c**) LTGC: total HR in *Slx4*$^{+/+}$ clones and *Slx4*$^{\Delta 125/\Delta}$ clones. Data

shows mean values, n=6. Error bars: s.e.m. Analysis by ANOVA. P-value *p < 0.05 and ****p < 0.0001 **d.** CRISPR/Cas9 with dual sgRNA targeting to generate *Slx4*$^{+/-}$ hemizygous cells. The *Slx4*$^{-}$ allele contains a 19.3kb deletion between exons 2 and 15. Red half arrowheads: PCR and sequencing primers specific to Exons 2 and 15. Predicted PCR product sizes for *Slx4*$^{+}$ (wild type) allele shown. **e.** Gel shows PCR products detected using gDNA from *Slx4*$^{+/+}$ and *Slx4*$^{+/-}$ clones. Note the 444 bp PCR product formed across the 19.3kb deletion between exons 2 and 15 in *Slx4*$^{+/-}$ cells. **f**. DNA sequencing chromatogram of PCR products from (**e**). **g**. RT qPCR analysis of *Slx4* mRNA in *Slx4*$^{+/+}$ and *Slx4*$^{+/-}$ cells. Data shows mean of three independent experiments (n=3) normalized to *Gapdh* mRNA using the $2^{-\Delta\Delta CT}$ method and analyzed by unpaired Student's *t*-test. Error bars: s.d.. **h**. and **i**. Quantification of colony formation of *Slx4*$^{+/+}$ *vs.* *Slx4*$^{+/-}$ clones in the presence of MMC (**h**), Olaparib (**i**). Data shows mean of three biologically independent replicates, n=3. Error bars: s.d. **j**. Tus/*Ter*-induced and I-SceI-induced repair frequencies in *Slx4*$^{+/+}$ and *Slx4*$^{+/-}$ cells. Data shows mean values of five biologically independent replicates, n=5. Error bars: s.e.m. Statistical analysis using ANOVA.

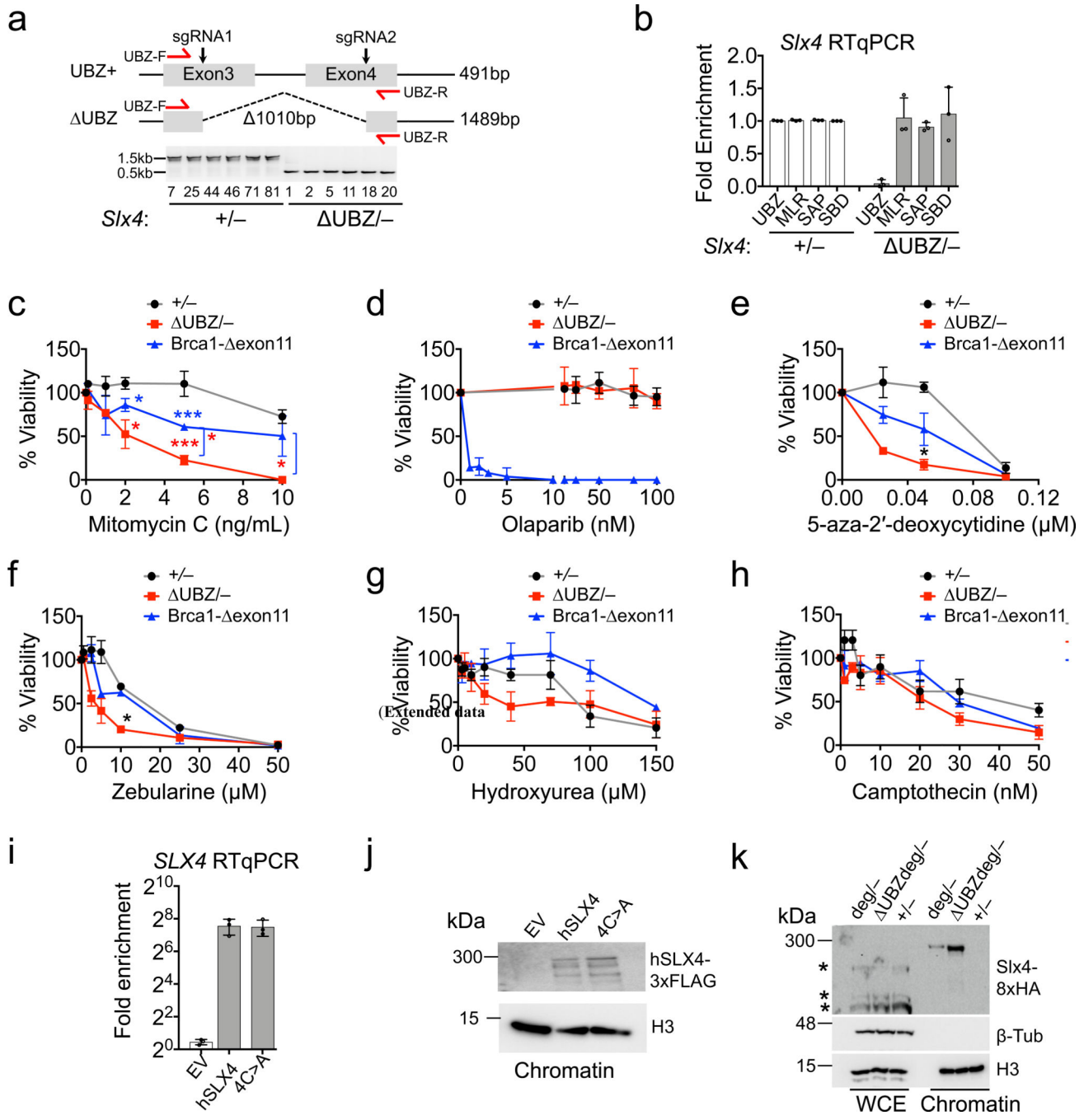

Extended Data Fig. 2. The SLX4 UBZ domain promotes resistance to DPC-inducing drugs

a. Strategy for in-frame deletion of UBZ domain-encoding regions of *Slx4*. Red half-arrow heads: genotyping PCR primers. Gel shows PCR products using gDNA from $Slx4^{+/-}$ and $Slx4^{\Delta UBZ/-}$ clones. Sequencing chromatogram shows in-frame breakpoint of $Slx4^{\Delta UBZ}$ allele. **b**. RT-qPCR analysis of mRNA encoding UBZ, MLR, SAP and SBD domains in $Slx4^{+/-}$ and $Slx4^{\Delta UBZ/-}$clones. Data normalized to *Gapdh* mRNA using the $2^{-\Delta CT}$ method, mRNA expression in $Slx4^{\Delta UBZ/-}$ samples were normalized to $Slx4^{+/-}$ of the same experiment. Each data point is an average of three technical replicates. Data shows mean of

three independent biological replicates (n=3). Analysis by unpaired Student's *t*-test (n=3). Error bars: standard deviation. P=0.0125 for mRNA expression of the UBZ region in *Slx4*$^{+/-}$ compared to *Slx4*$^{\Delta UBZ/-}$. No significant differences were observed in expression levels of all other domains. **c**-**h**. Quantification of colony formation of *Slx4*$^{+/-}$, *Slx4*$^{\Delta UBZ/-}$ and Brca1-Δexon11 clones in the presence of MMC (**c**), Olaparib (**d**), 5-aza-2′-deoxycytidine (**e**) Zebularine (**f**), Hydroxyurea (**g**) and Camptothecin (**h**). Data shows mean of values of three biologically independent replicates, n=3. Analysis using Student's *t*-test. P-value *p < 0.05 and ***p < 0.001. Red asterisks refer to comparison between *Slx4*$^{+/-}$ and *Slx4*$^{\Delta UBZ/-}$ clones; blue asterisks denote comparison between *Slx4*$^{+/-}$ and Brca1-Δexon11 clones and blue bracket with red asterisks denotes comparison between *Slx4*$^{\Delta UBZ/-}$ and Brca1-Δexon11 clones. Error bars: s.d. **i**. RT-qPCR analysis of N-terminal Flag-tagged wild-type full-length human SLX4 and UBZ 4C>A expression plasmids 48h after transfection. Data normalized to *Gapdh* mRNA using the $2^{-\Delta CT}$ method and compared to empty vector (EV) control. Each data point is an average of three technical replicates. Data shows mean of three independent biological replicates (n=3). Error bar: s.d. **j**. Western blot analysis of the chromatin-bound fraction of various human 3xFLAG-SLX4 full-length and UBZ 4C>A transiently expressed for 48 hours and blotted with anti-FLAG antibody. **k**. Western blot analysis of whole cell extract (WCE) and chromatin-bound fraction of clones of *Slx4*$^{+/-}$ and *Slx4*$^{\Delta UBZ/-}$ tagged with a dual degron containing a C-terminal 8xHA tag and untagged hemizygote cells (+/–). Asterisk (*) denotes non-specific bands.

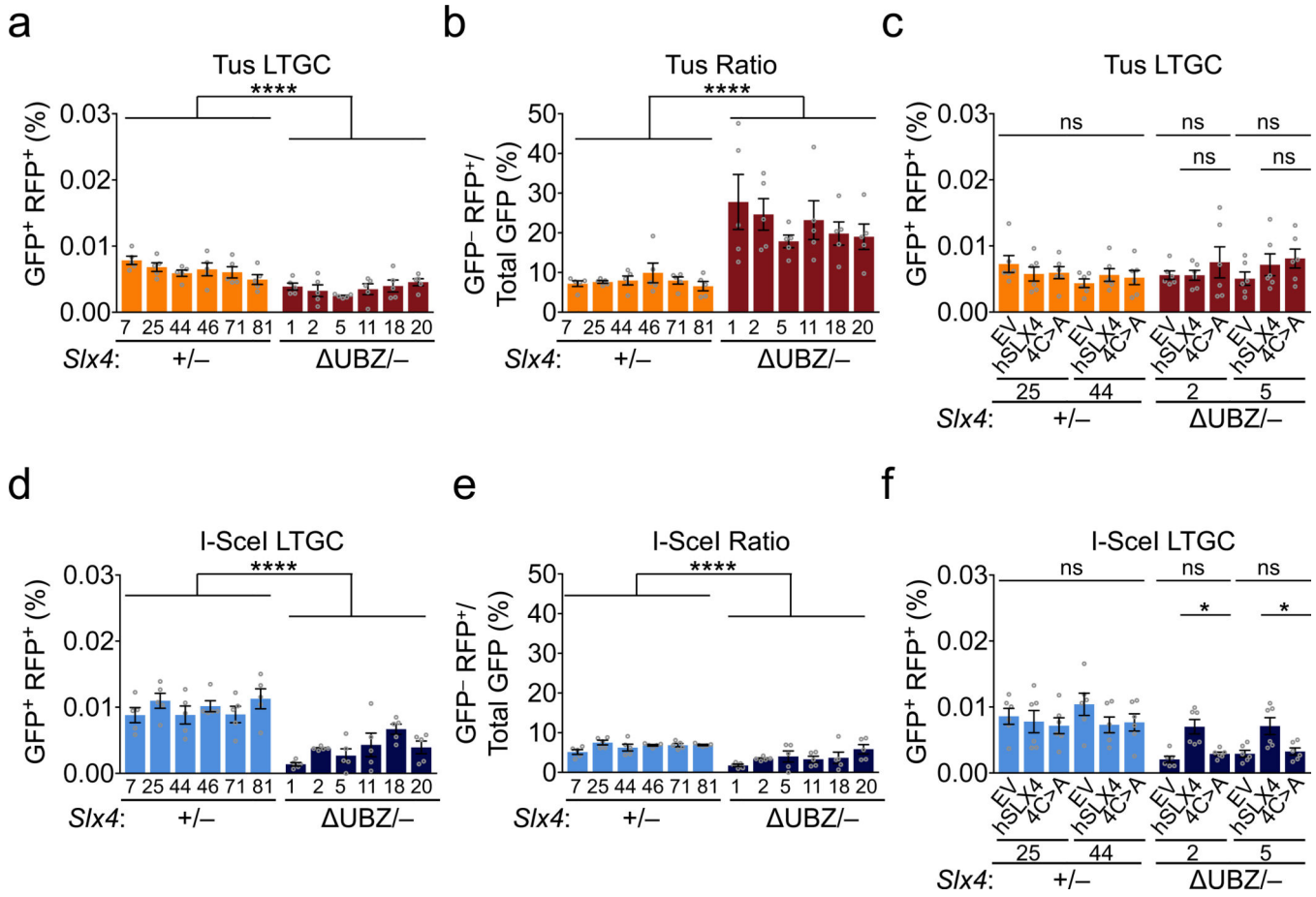

Extended Data Fig. 3. The SLX4 UBZ domain mediates I-SceI-induced LTGC

a and **b**. Tus/*Ter*-induced LTGC (**a**) and LTGC/Total HR ratio (**b**) in *Slx4*$^{+/-}$ and *Slx4*$^{\Delta UBZ/-}$ clones. Data shows mean values of five biologically independent replicates, n=5. Error bars: s.e.m. Analysis by one-way ANOVA. P-value: ****p < 0.0001. Error bars: s.e.m. **c**. Impact of exogenous h*SLX4* on Tus/*Ter*-induced LTGC in two independent *Slx4*$^{+/-}$ and two independent *Slx4*$^{\Delta UBZ/-}$ clones. EV: empty vector. 4C>A: h*SLX4* with inactivated UBZ motifs. Data shows mean values of five biologically independent replicates, n=6. Error bars: s.e.m. Analysis by unpaired Student's *t*-test. Error bars: s.e.m. **d** and **e**. I-SceI-induced LTGC (**d**) and LTGC/Total HR ratio (**e**) in *Slx4*$^{+/-}$ and *Slx4*$^{\Delta UBZ/-}$ clones. Data shows mean values of five biologically independent replicates, n=5. P-value: ****p < 0.0001 Error bars: s.e.m. Analysis by one-way ANOVA. Error bars: s.e.m. **f**. Impact of exogenous h*SLX4* on I-SceI-induced LTGC in two independent *Slx4*$^{+/-}$ and two independent *Slx4*$^{\Delta UBZ/-}$ clones. EV: empty vector. 4C>A: h*SLX4* with inactivated UBZ motifs. Data shows mean values of six biologically independent replicates, n=6. Error bars: s.e.m. Analysis by unpaired Student's *t*-test. P-value: *p < 0.05. Error bars: s.e.m.

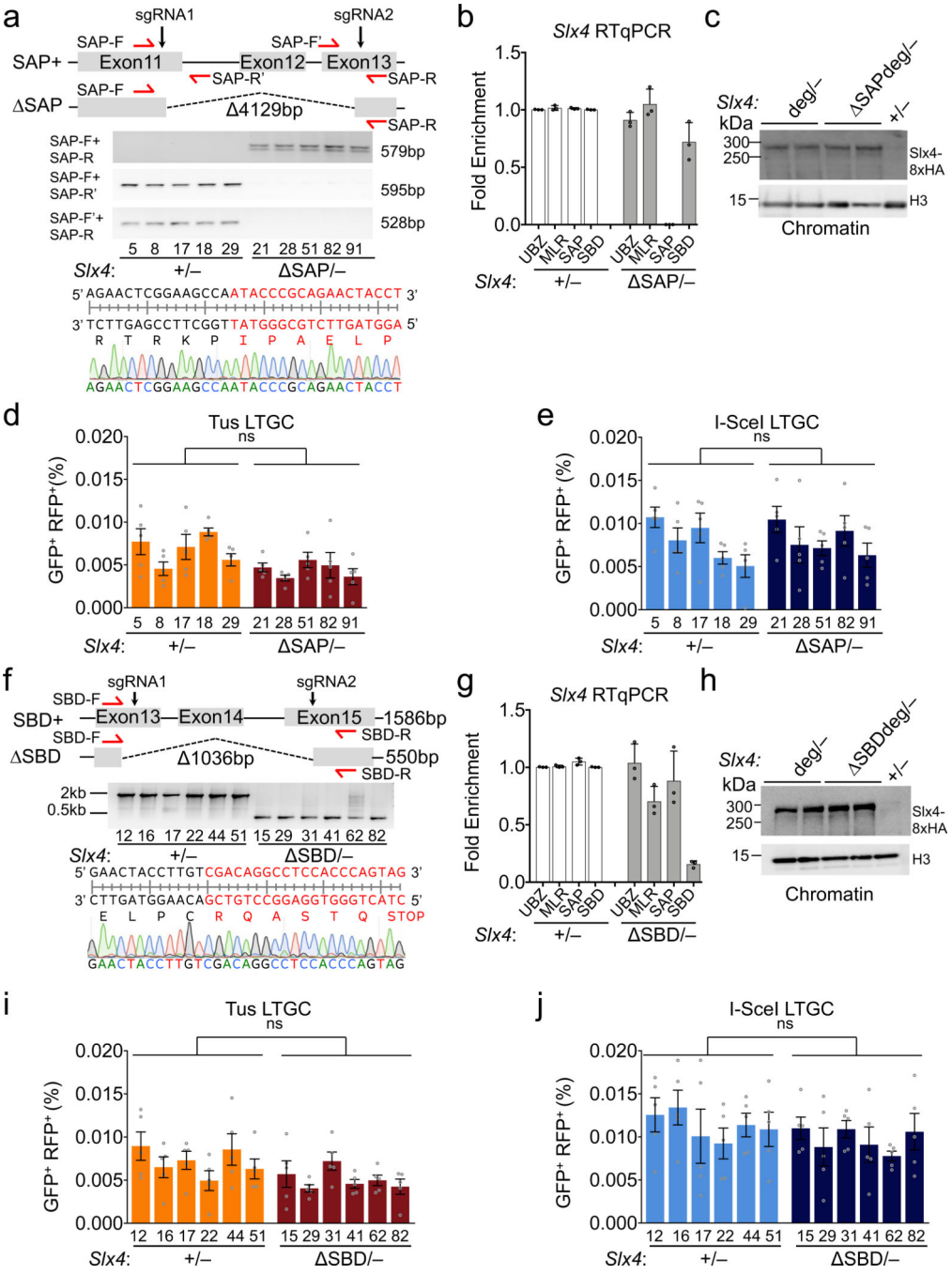

Extended Data Fig. 4. Characterization of *Slx4*$^{\Delta SAP/-}$ and *Slx4*$^{\Delta SBD/-}$ mutant clones

a. Strategy for in-frame deletion of SAP domain-encoding region of *Slx4*. Red half-arrow heads: genotyping PCR primers. Gels show PCR products using gDNA from *Slx4*$^{+/-}$ and *Slx4*$^{\Delta SAP/-}$ clones. Sequencing chromatogram shows in-frame breakpoint of *Slx4*$^{\Delta SAP}$ allele. **b**. RT-qPCR analysis of UBZ, MLR, SAP and SBD domains encoding mRNA in *Slx4*$^{+/-}$ and *Slx4*$^{\Delta SAP/-}$clones. Data normalized to *Gapdh* mRNA using the $2^{-\Delta CT}$ method, mRNA expression in *Slx4*$^{\Delta SAP/-}$ were normalized to *Slx4*$^{+/-}$. Each data point is an average of three technical replicates. Data shows mean of three independent biological

replicates (n=3). Analysis by unpaired Student's *t*-test. Error bars: s.d. P=0.0478 for mRNA expression of the SAP region in *Slx4*$^{+/-}$ compared to *Slx4*$^{\Delta SAP/-}$. No significant differences were observed in expression levels of all other domains. **c**. Anti-HA immunoblot of two independent HA-degron tagged *Slx4*$^{\Delta SAP/-}$ and *Slx4*$^{+/-}$ isogenic cell lines. The parental *Slx4*$^{+/-}$ untagged cell line was used as a control. **d** and **e**. Tus/*Ter*-induced LTGC (**d**) and I-SceI-induced LTGC (**e**) in *Slx4*$^{+/-}$ and *Slx4*$^{\Delta SAP/-}$ clones. Data shows mean values of five biologically independent replicates, n=5. Error bars: s.e.m. Analysis by ordinary one-way ANOVA. Error bars: s.e.m. **f**. Strategy for in-frame deletion of SBD domain-encoding region of *Slx4*. Red half-arrow heads: genotyping PCR primers. Gels show PCR products using gDNA from *Slx4*$^{+/-}$ and *Slx4*$^{\Delta SBD/-}$ clones. Sequencing chromatogram shows in-frame breakpoint of *Slx4*$^{\Delta SBD}$ allele. **g**. RT-qPCR analysis of UBZ, MLR, SAP and SBD domains encoding mRNA in *Slx4*$^{+/-}$ and *Slx4*$^{\Delta SBD/-}$clones. Data normalized to *Gapdh* mRNA using the $2^{-\Delta CT}$ method, mRNA expression in *Slx4*$^{\Delta SBD/-}$ was normalized to *Slx4*$^{+/-}$ of the same experiment. Each data point is an average of three technical replicates. Data shows mean of three independent biological replicates (n=3). Analysis by unpaired Student's *t*-test (n=3). Error bars: standard deviation. P=0.048 for mRNA expression of the SAP region in *Slx4*$^{+/-}$ compared to *Slx4*$^{\Delta SBD/-}$. No significant differences were observed in expression levels of all other domains. **h**. Anti-HA immunoblot of two independent HA-degron tagged *Slx4*$^{\Delta SBD/-}$ and *Slx4*$^{+/-}$ isogenic cell lines. The parental *Slx4*$^{+/-}$ untagged cell line was used as a control. **i** and **j**. Tus/*Ter*-induced LTGC (**i**) and I-SceI-induced LTGC (**j**) in *Slx4*$^{+/-}$ and *Slx4*$^{\Delta SBD/-}$ clones. Data shows mean values of five biologically independent replicates, n=5. Error bars: s.e.m. Analysis by ordinary one-way ANOVA. Error bars: s.e.m.

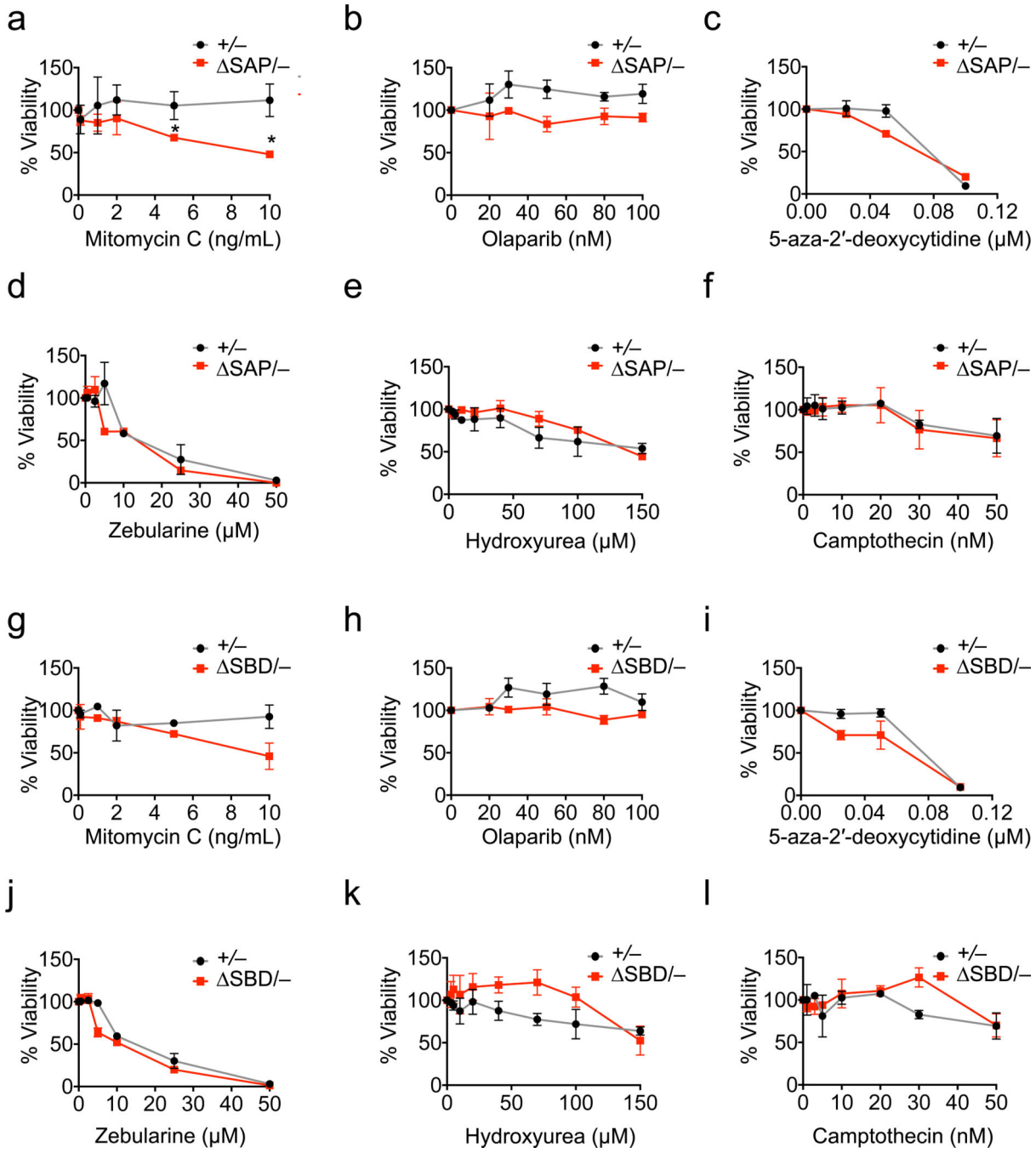

Extended Data Fig. 5. *Slx4*$^{\Delta SAP/-}$ and *Slx4*$^{\Delta SBD/-}$ mutant clones are resistant to DPC-inducing drugs

a-f. Quantification of colony formation of *Slx4*$^{+/-}$ *vs.* *Slx4*$^{\Delta SAP/-}$ clones in the presence of MMC (**a**), Olaparib (**b**), 5-aza-2′-deoxycytidine (**c**), Zebularine (**d**) Hydroxyurea (**e**) and Camptothecin (**f**). Data show mean of three biologically independent replicates normalized to untreated samples (n=3). Error bars: s.d. **g-l**. Quantification of colony formation of *Slx4*$^{+/-}$ *vs.* *Slx4*$^{\Delta SBD/-}$ clones in the presence of MMC (**g**), Olaparib (**h**), 5-aza-2′-deoxycytidine (**i**), Zebularine (**j**) Hydroxyurea (**k**) and Camptothecin (**l**). Data show mean of

three biologically independent replicates normalized to untreated samples (n=3). Error bars: s.d.

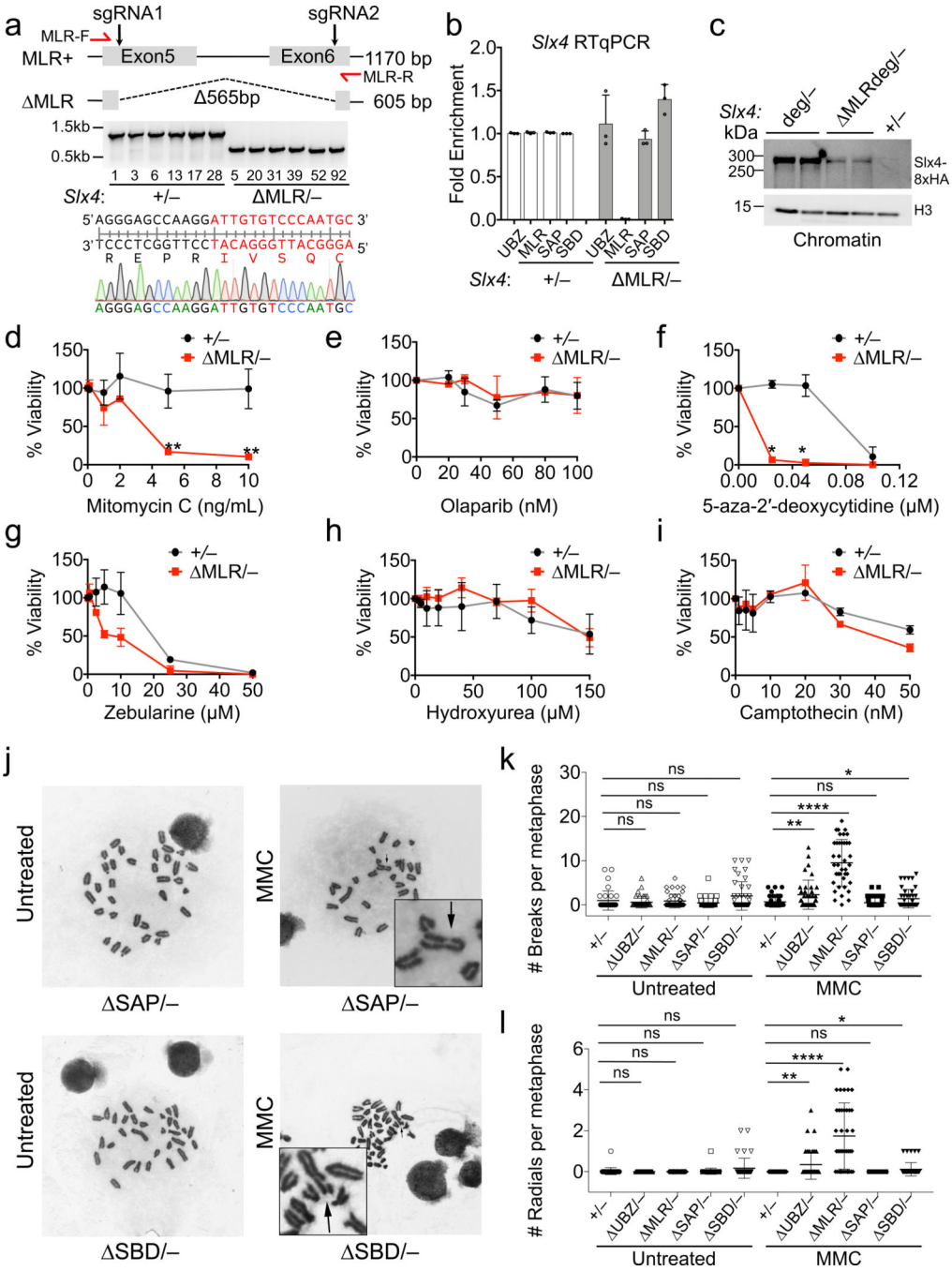

Extended Data Fig. 6. Characterization of *Slx4*$^{\Delta MLR/-}$ mutant clones

a. Strategy for in-frame deletion of MLR domain-encoding region of *Slx4*. Red half-arrow heads: genotyping PCR primers. Gels show PCR products using gDNA from *Slx4*$^{+/-}$ and *Slx4*$^{\Delta MLR/-}$ clones. Sequencing chromatogram shows in-frame breakpoint of *Slx4*$^{\Delta MLR}$ allele. **b**. RT-qPCR analysis of UBZ, MLR, SAP and SBD domains encoding mRNA in

Slx4$^{+/-}$ and *Slx4*$^{\Delta MLR/-}$clones. Data normalized to *Gapdh* mRNA using the $2^{-\Delta CT}$ method, mRNA expression in *Slx4*$^{\Delta MLR/-}$ were normalized to *Slx4*$^{+/-}$ of the same experiment. Each data point is an average of three technical replicates. Data shows mean of three independent biological replicates (n=3). Analysis by unpaired Student's *t*-test (n=3). Error bars: standard deviation (s.d.). P=0.01 for mRNA expression of the MLR region in *Slx4*$^{+/-}$ compared to *Slx4*$^{\Delta MLR/-}$. No significant differences were observed in expression levels of all other domains. **c** Anti-HA immunoblot of two independent HA-degron tagged *Slx4*$^{\Delta MLR/-}$ and *Slx4*$^{+/-}$ isogenic cell lines. The parental *Slx4*$^{+/-}$ untagged cell line was used as a control. **d**-**g**. Quantification of cell survival assays of *Slx4*$^{+/-}$ and *Slx4*$^{\Delta MLR/-}$ clones in the presence of MMC (**d**), Olaparib (**e**) 5-aza-2′-deoxycytidine (**f**) Zebularine (**g**), Hydroxyurea (**h**) and Camptothecin (**i**). Data show mean values of three biologically independent replicates, n=3. P-value: *p < 0.05. Analysis using unpaired Student's *t*-test. Error bars: s.d. **j**. Representative images of metaphase spreads showing chromatid breaks (black arrows) and radial chromosomes (black arrowheads) in cells either untreated or treated with 20 ng/mL MMC for 12h in *Slx4*$^{\Delta SAP/-}$ and *Slx4*$^{\Delta SBD/-}$ cells. **k.** and **l**. Quantitation of the number of breaks (**k**) and radial chromosomes (**l**) per metaphase nucleus in *Slx4* mutant cells shown. Treated and untreated cells were harvested at the same time and each sample represented one independent experiment, n=1. Data shows mean values of breaks or radials per genotype. Analysis using unpaired Student's *t*-test. P-value: ****p < 0.0001.

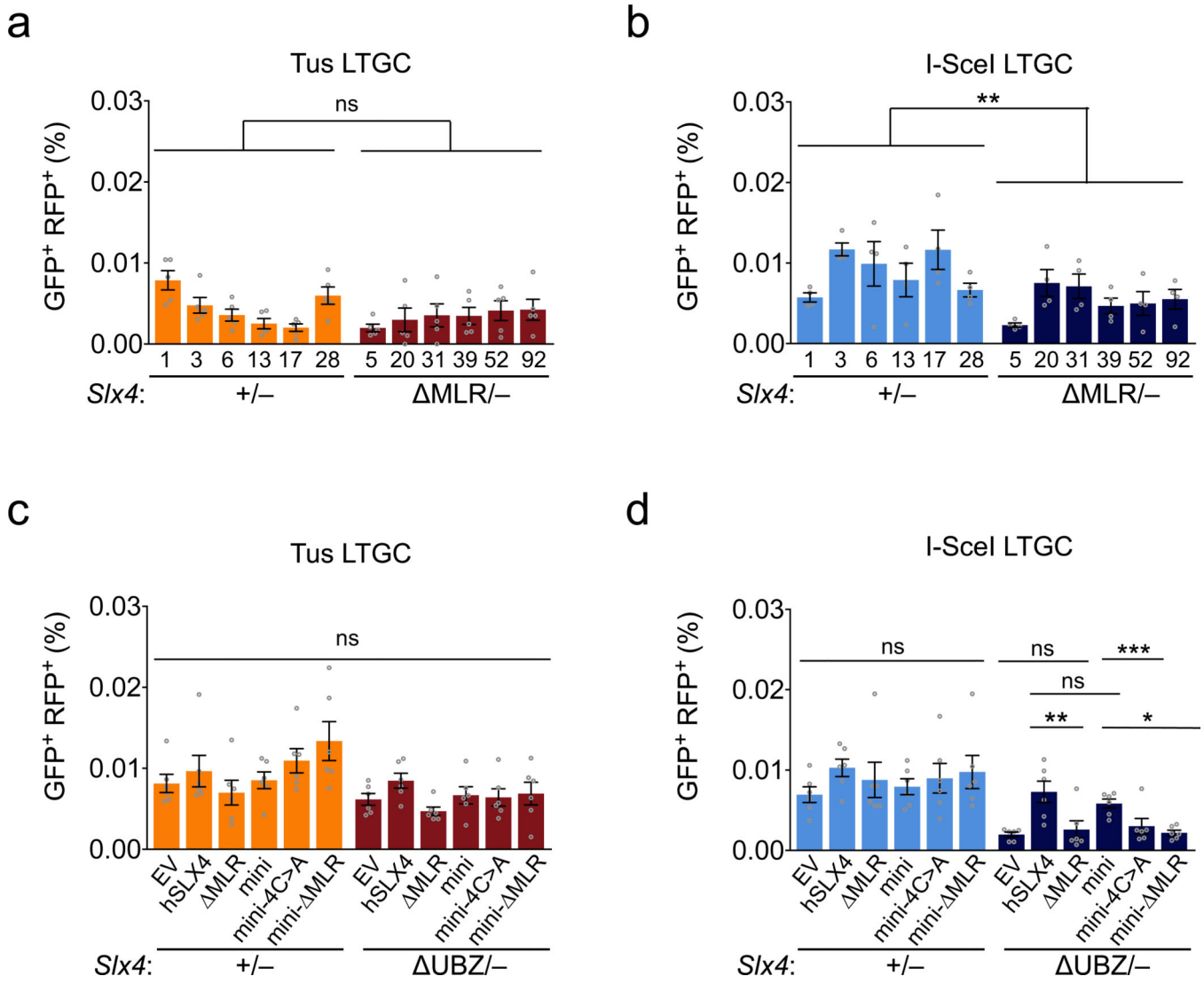

Extended Data Fig. 7. The SLX4 MLR domain contributes to I-SceI-induced LTGC

a and **b**. Tus/*Ter*-induced LTGC (**a**) and I-SceI-induced LTGC (**b**) in *Slx4*$^{+/-}$ and *Slx4*$^{\Delta MLR/-}$ clones. Data shows mean values of five biologically independent replicates, n=5. P-value: **p < 0.01. Error bars: s.e.m. Analysis by ordinary one-way ANOVA. Error bars: s.e.m. **c** and **d**. Impact of exogenous h*SLX4* alleles (see Fig. 5c) on Tus/*Ter*-induced LTGC (**c**) and on I-SceI-induced LTGC (**d**) in *Slx4*$^{+/-}$ and *Slx4*$^{\Delta UBZ/-}$ clones. EV: empty vector. 4C>A: h*SLX4* with inactivated UBZ motifs. Data shows mean values of six biologically independent replicates, n=6. P-value: *p < 0.05; **p < 0.01; ***p < 0.00. Error bars: s.e.m. Analysis by unpaired Student's *t*-test.

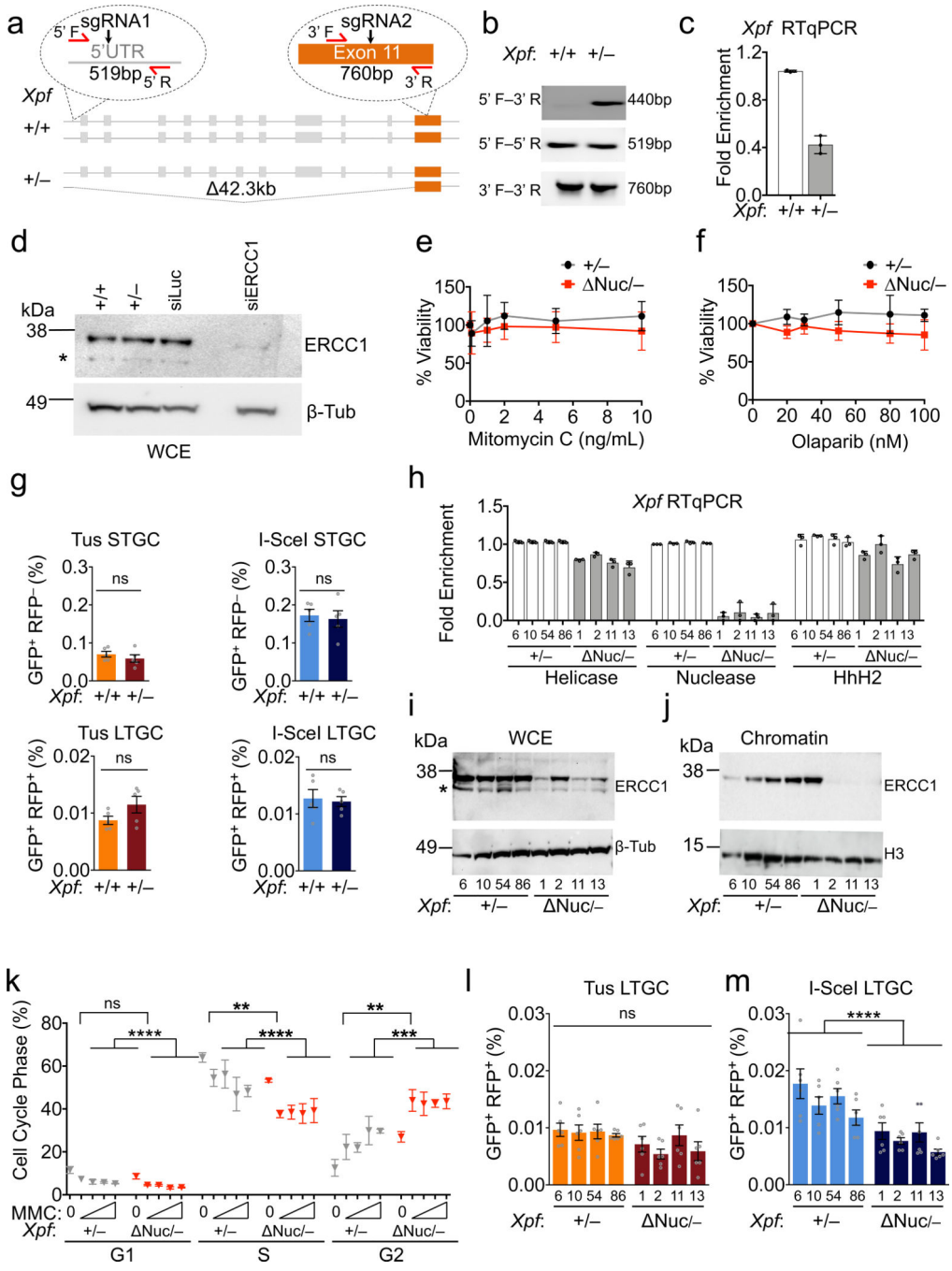

Extended Data Fig. 8. Characterization of *Xpf*$^{+/-}$ and *Xpf*$^{\Delta Nuc/-}$ cells

a. CRISPR/Cas9 with dual sgRNA strategy for generation of *Xpf*$^{+/-}$ hemizygous cells. The *Xpf*$^{-}$ allele contains a 42.3 kb deletion between the 5'UTR and exon 11. Red half arrowheads: PCR and sequencing primers specific to 5'UTR and Exon 11. Predicted PCR product sizes for *Xpf*$^{+}$ (wild type) allele shown. **b.** Gel shows PCR products using gDNA from *Xpf*$^{+/+}$ and *Xpf*$^{+/-}$ clones. Note the 440 bp PCR product formed across the 42.3kb deletion between the 5'UTR and exon 11 in *Xpf*$^{+/-}$ cells. **c**. RT qPCR analysis of mRNA in *Xpf*$^{+/+}$ and *Xpf*$^{+/-}$ cells. Data shows mean of three independent experiments

(n=3) normalized to *Gapdh* mRNA using the $2^{-\Delta\Delta CT}$ method and analyzed by unpaired Student's *t*-test. Error bars: s.d. **d**. Western blot of whole cell lysates in $Xpf^{+/+}$ or $Xpf^{+/-}$ clones. siLuc and siErcc1 were compared in $Xpf^{+/-}$ cell line 48 hours after transfection to validate specificity of the Ercc1 band. **e**. and **f**. Quantification of colony formation of $Xpf^{+/+}$ *vs.* $Xpf^{+/-}$ clones in the presence of MMC (**e**), Olaparib (**f**). Data show mean values of three biologically independent replicates, n=3. Error bars: s.d. **g**. Tus/*Ter*-induced and I-SceI-induced HR frequencies in $Xpf^{+/+}$ or $Xpf^{+/-}$ clones. Data shows mean values of four biologically independent replicates, n=4. Error bars: s.e.m. Analysis by unpaired Student's *t*-test. Error bars: s.e.m **h**. RT-qPCR analysis of mRNA encoding the XPF helicase, nuclease and Hh2h domains in 4 isogenic $Xpf^{+/-}$ clones and 4 $Xpf^{\Delta Nuc/-}$ clones. Data normalized to *Gapdh* mRNA using the $2^{-\Delta CT}$ method, mRNA expression in $Xpf^{\Delta Nuc/-}$ was normalized to $Xpf^{+/-}$ of the same experiment. Each data point is an average of three technical replicates. Data shows mean of three independent biological replicates (n=3). Analysis by unpaired Student's *t*-test. Error bars: s.d. P=0.0153 for mRNA expression of the Nuclease region in $Xpf^{+/-}$ compared to $Xpf^{\Delta Nuc/-}$. No significant differences were observed in expression levels of all other domains. **i**. Western blot analysis of ERCC1 in whole cell extract (WCE). *: non-specific band. β-tubulin: Loading control. **j**. Western blot analysis of ERCC1 in chromatin fraction of $Xpf^{+/-}$ and $Xpf^{\Delta Nuc/-}$ clones. H3: Histone H3 loading control. Note presence of ERCC1 signal in in-frame deleted $Xpf^{\Delta Nuc/-}$ clone #1, and absence of ERCC1 signal in frame-shifted $Xpf^{\Delta Nuc/-}$ clones #2, 11 and 13 **k**. Cell cycle distribution of $Xpf^{+/-}$ clone #6 and $Xpf^{\Delta Nuc/-}$ clone #1, either untreated or treated with 20, 30, 40 or 50 ng/mL of MMC. Data shows mean values of three biologically independent replicates, n=3. P-value: **p < 0.01; ***p < 0.001; ****p < 0.0001. Error bars: s.e.m. Untreated samples were compared using the unpaired Student's *t*-test; MMC-treated groups were compared by one-way ANOVA. **l** and **m**. Tus/*Ter*-induced LTGC (**l**) and I-SceI induced LTGC (**m**) in $Xpf^{+/-}$ and $Xpf^{\Delta Nuc/-}$ clones. Data shows mean values of six biologically independent replicates, n=6. Error bars: s.e.m. Analysis by ordinary one-way ANOVA. P-value: ****p < 0.0001.

Supplementary Material

Refer to Web version on PubMed Central for supplementary material.

Acknowledgements

We thank Drs. Johannes Walter and Ketan J. Patel for helpful discussions and expert advice. This work was supported by grants R01GM134425 (to R.S.) and R01CA204127 (to A.S.), and by AACR fellowship 19-40-12-PAND (to A.P.). A.S. is a Howard Hughes Faculty Scholar.

Data Availability

All data supporting the findings of this study are available from the corresponding author upon request. Source data are provided with this paper.

References

1. Berti M, Cortez D. & Lopes M. The plasticity of DNA replication forks in response to clinically relevant genotoxic stress. Nat Rev Mol Cell Biol 21, 633–651 (2020). [PubMed: 32612242]

2. Cortez D. Replication-Coupled DNA Repair. Mol Cell 74, 866–876 (2019). [PubMed: 31173722]
3. Quinet A, Tirman S, Cybulla E, Meroni A. & Vindigni A. To skip or not to skip: choosing repriming to tolerate DNA damage. Mol Cell 81, 649–658 (2021). [PubMed: 33515486]
4. Crossley MP, Bocek M. & Cimprich KA R-Loops as Cellular Regulators and Genomic Threats. Mol Cell 73, 398–411 (2019). [PubMed: 30735654]
5. Semlow DR, Zhang J, Budzowska M, Drohat AC & Walter JC Replication-Dependent Unhooking of DNA Interstrand Cross-Links by the NEIL3 Glycosylase. Cell 167, 498–511 e14 (2016). [PubMed: 27693351]
6. Hodskinson MR et al. Alcohol-derived DNA crosslinks are repaired by two distinct mechanisms. Nature 579, 603–608 (2020). [PubMed: 32132710]
7. Huang J. et al. The DNA translocase FANCM/MHF promotes replication traverse of DNA interstrand crosslinks. Mol Cell 52, 434–46 (2013). [PubMed: 24207054]
8. Huang J. et al. Remodeling of Interstrand Crosslink Proximal Replisomes Is Dependent on ATR, FANCM, and FANCD2. Cell Rep 27, 1794–1808.e5 (2019). [PubMed: 31067464]
9. Semlow DR & Walter JC Mechanisms of Vertebrate DNA Interstrand Cross-Link Repair. Annu Rev Biochem (2021).
10. Niraj J, Färkkilä A. & D'Andrea AD The Fanconi Anemia Pathway in Cancer. Annu Rev Cancer Biol 3, 457–478 (2019). [PubMed: 30882047]
11. Taylor AMR et al. Chromosome instability syndromes. Nat Rev Dis Primers 5, 64 (2019). [PubMed: 31537806]
12. Garaycoechea JI et al. Alcohol and endogenous aldehydes damage chromosomes and mutate stem cells. Nature 553, 171–177 (2018). [PubMed: 29323295]
13. Langevin F, Crossan GP, Rosado IV, Arends MJ & Patel KJ Fancd2 counteracts the toxic effects of naturally produced aldehydes in mice. Nature 475, 53–8 (2011). [PubMed: 21734703]
14. Rosado IV, Langevin F, Crossan GP, Takata M. & Patel KJ Formaldehyde catabolism is essential in cells deficient for the Fanconi anemia DNA-repair pathway. Nat Struct Mol Biol 18, 1432–4 (2011). [PubMed: 22081012]
15. O'Brien PJ, Siraki AG & Shangari N. Aldehyde sources, metabolism, molecular toxicity mechanisms, and possible effects on human health. Crit Rev Toxicol 35, 609–62 (2005). [PubMed: 16417045]
16. Raschle M. et al. Mechanism of replication-coupled DNA interstrand crosslink repair. Cell 134, 969–80 (2008). [PubMed: 18805090]
17. Wu RA et al. TRAIP is a master regulator of DNA interstrand crosslink repair. Nature 567, 267–272 (2019). [PubMed: 30842657]
18. Wang S, Wang R, Peralta C, Yaseen A. & Pavletich NP Structure of the FA core ubiquitin ligase closing the ID clamp on DNA. Nat Struct Mol Biol 28, 300–309 (2021). [PubMed: 33686268]
19. Shakeel S. et al. Structure of the Fanconi anaemia monoubiquitin ligase complex. Nature 575, 234–237 (2019). [PubMed: 31666700]
20. Xue X, Sung P. & Zhao X. Functions and regulation of the multitasking FANCM family of DNA motor proteins. Genes Dev 29, 1777–88 (2015). [PubMed: 26341555]
21. Alcón P. et al. FANCD2-FANCI is a clamp stabilized on DNA by monoubiquitination of FANCD2 during DNA repair. Nat Struct Mol Biol 27, 240–248 (2020). [PubMed: 32066963]
22. Tan W. et al. Monoubiquitination by the human Fanconi anemia core complex clamps FANCI:FANCD2 on DNA in filamentous arrays. Elife 9(2020).
23. Amunugama R. et al. Replication Fork Reversal during DNA Interstrand Crosslink Repair Requires CMG Unloading. Cell Rep 23, 3419–3428 (2018). [PubMed: 29924986]
24. Kim Y. et al. Regulation of multiple DNA repair pathways by the Fanconi anemia protein SLX4. Blood 121, 54–63 (2013). [PubMed: 23093618]
25. Klein Douwel D. et al. XPF-ERCC1 acts in Unhooking DNA interstrand crosslinks in cooperation with FANCD2 and FANCP/SLX4. Mol Cell 54, 460–71 (2014). [PubMed: 24726325]
26. Bogliolo M. et al. Mutations in ERCC4, encoding the DNA-repair endonuclease XPF, cause Fanconi anemia. Am J Hum Genet 92, 800–6 (2013). [PubMed: 23623386]

27. Marín M. et al. Functional Comparison of XPF Missense Mutations Associated to Multiple DNA Repair Disorders. Genes (Basel) 10(2019).
28. Hodskinson MR et al. Mouse SLX4 is a tumor suppressor that stimulates the activity of the nuclease XPF-ERCC1 in DNA crosslink repair. Mol Cell 54, 472–84 (2014). [PubMed: 24726326]
29. Manandhar M, Boulware KS & Wood RD The ERCC1 and ERCC4 (XPF) genes and gene products. Gene 569, 153–61 (2015). [PubMed: 26074087]
30. Zhang J. & Walter JC Mechanism and regulation of incisions during DNA interstrand cross-link repair. DNA Repair (Amst) 19, 135–42 (2014). [PubMed: 24768452]
31. Duxin JP & Walter JC What is the DNA repair defect underlying Fanconi anemia? Curr Opin Cell Biol 37, 49–60 (2015). [PubMed: 26512453]
32. Willis NA et al. BRCA1 controls homologous recombination at Tus/Ter-stalled mammalian replication forks. Nature 510, 556–9 (2014). [PubMed: 24776801]
33. Willis NA et al. Mechanism of tandem duplication formation in BRCA1-mutant cells. Nature 551, 590–595 (2017). [PubMed: 29168504]
34. Nik-Zainal S. et al. Landscape of somatic mutations in 560 breast cancer whole-genome sequences. Nature 534, 47–54 (2016). [PubMed: 27135926]
35. Menghi F. et al. The Tandem Duplicator Phenotype Is a Prevalent Genome-Wide Cancer Configuration Driven by Distinct Gene Mutations. Cancer Cell 34, 197–210 e5 (2018). [PubMed: 30017478]
36. Scully R, Panday A, Elango R. & Willis NA DNA double-strand break repair-pathway choice in somatic mammalian cells. Nat Rev Mol Cell Biol 20, 698–714 (2019). [PubMed: 31263220]
37. Panday A. et al. FANCM regulates repair pathway choice at stalled replication forks. Mol Cell (2021).
38. Lambert S. et al. Homologous recombination restarts blocked replication forks at the expense of genome rearrangements by template exchange. Mol Cell 39, 346–59 (2010). [PubMed: 20705238]
39. Wyatt HD, Laister RC, Martin SR, Arrowsmith CH & West SC The SMX DNA Repair Tri-nuclease. Mol Cell 65, 848–860 e11 (2017). [PubMed: 28257701]
40. Fekairi S. et al. Human SLX4 is a Holliday junction resolvase subunit that binds multiple DNA repair/recombination endonucleases. Cell 138, 78–89 (2009). [PubMed: 19596236]
41. Svendsen JM et al. Mammalian BTBD12/SLX4 assembles a Holliday junction resolvase and is required for DNA repair. Cell 138, 63–77 (2009). [PubMed: 19596235]
42. Saito TT, Youds JL, Boulton SJ & Colaiácovo MP Caenorhabditis elegans HIM-18/SLX-4 interacts with SLX-1 and XPF-1 and maintains genomic integrity in the germline by processing recombination intermediates. PLoS Genet 5, e1000735 (2009). [PubMed: 19936019]
43. Andersen SL et al. Drosophila MUS312 and the vertebrate ortholog BTBD12 interact with DNA structure-specific endonucleases in DNA repair and recombination. Mol Cell 35, 128–35 (2009). [PubMed: 19595722]
44. Guervilly JH & Gaillard PH SLX4: multitasking to maintain genome stability. Crit Rev Biochem Mol Biol 53, 475–514 (2018). [PubMed: 30284473]
45. Young SJ & West SC Coordinated roles of SLX4 and MutSβ in DNA repair and the maintenance of genome stability. Crit Rev Biochem Mol Biol 56, 157–177 (2021). [PubMed: 33596761]
46. Young SJ et al. MutSbeta Stimulates Holliday Junction Resolution by the SMX Complex. Cell Rep 33, 108289 (2020). [PubMed: 33086055]
47. Kim Y. et al. Mutations of the SLX4 gene in Fanconi anemia. Nat Genet 43, 142–6 (2011). [PubMed: 21240275]
48. Lachaud C. et al. Distinct functional roles for the two SLX4 ubiquitin-binding UBZ domains mutated in Fanconi anemia. J Cell Sci 127, 2811–7 (2014). [PubMed: 24794496]
49. Katsuki Y. et al. RNF168 E3 ligase participates in ubiquitin signaling and recruitment of SLX4 during DNA crosslink repair. Cell Rep 37, 109879 (2021). [PubMed: 34706224]
50. Stoepker C. et al. SLX4, a coordinator of structure-specific endonucleases, is mutated in a new Fanconi anemia subtype. Nat Genet 43, 138–41 (2011). [PubMed: 21240277]
51. Crossan GP et al. Disruption of mouse Slx4, a regulator of structure-specific nucleases, phenocopies Fanconi anemia. Nat Genet 43, 147–52 (2011). [PubMed: 21240276]

52. Yamamoto KN et al. Involvement of SLX4 in interstrand cross-link repair is regulated by the Fanconi anemia pathway. Proc Natl Acad Sci U S A 108, 6492–6 (2011). [PubMed: 21464321]
53. Kosicki M, Tomberg K. & Bradley A. Repair of double-strand breaks induced by CRISPR-Cas9 leads to large deletions and complex rearrangements. Nat Biotechnol 36, 765–771 (2018). [PubMed: 30010673]
54. Jüttermann R, Li E. & Jaenisch R. Toxicity of 5-aza-2'-deoxycytidine to mammalian cells is mediated primarily by covalent trapping of DNA methyltransferase rather than DNA demethylation. Proc Natl Acad Sci U S A 91, 11797–801 (1994). [PubMed: 7527544]
55. Zhou L. et al. Zebularine: a novel DNA methylation inhibitor that forms a covalent complex with DNA methyltransferases. J Mol Biol 321, 591–9 (2002). [PubMed: 12206775]
56. Natsume T, Kiyomitsu T, Saga Y. & Kanemaki MT Rapid Protein Depletion in Human Cells by Auxin-Inducible Degron Tagging with Short Homology Donors. Cell Rep 15, 210–218 (2016). [PubMed: 27052166]
57. Nishimura K. et al. A super-sensitive auxin-inducible degron system with an engineered auxin-TIR1 pair. Nucleic Acids Res (2020).
58. Chung HK et al. Tunable and reversible drug control of protein production via a self-excising degron. Nat Chem Biol 11, 713–20 (2015). [PubMed: 26214256]
59. Wang X. et al. Role of DNA replication proteins in double-strand break-induced recombination in Saccharomyces cerevisiae. Mol Cell Biol 24, 6891–9 (2004). [PubMed: 15282291]
60. Willis NA et al. BRCA1 controls homologous recombination at Tus/Ter-stalled mammalian replication forks. Nature 510, 556-+ (2014).
61. Duxin JP, Dewar JM, Yardimci H. & Walter JC Repair of a DNA-protein crosslink by replication-coupled proteolysis. Cell 159, 346–57 (2014). [PubMed: 25303529]
62. Larsen NB et al. Replication-Coupled DNA-Protein Crosslink Repair by SPRTN and the Proteasome in Xenopus Egg Extracts. Mol Cell 73, 574–588.e7 (2019). [PubMed: 30595436]
63. Sparks JL et al. The CMG Helicase Bypasses DNA-Protein Cross-Links to Facilitate Their Repair. Cell 176, 167–181 e21 (2019). [PubMed: 30595447]
64. Stingele J, Bellelli R. & Boulton SJ Mechanisms of DNA-protein crosslink repair. Nat Rev Mol Cell Biol 18, 563–573 (2017). [PubMed: 28655905]
65. Wu W. et al. RTEL1 suppresses G-quadruplex-associated R-loops at difficult-to-replicate loci in the human genome. Nat Struct Mol Biol 27, 424–437 (2020). [PubMed: 32398827]
66. Di Marco S. et al. RECQ5 Helicase Cooperates with MUS81 Endonuclease in Processing Stalled Replication Forks at Common Fragile Sites during Mitosis. Mol Cell 66, 658–671.e8 (2017). [PubMed: 28575661]
67. Garribba L. et al. Folate stress induces SLX1- and RAD51-dependent mitotic DNA synthesis at the fragile X locus in human cells. Proc Natl Acad Sci U S A 117, 16527–16536 (2020). [PubMed: 32601218]

Methods-only references

68. Puget N, Knowlton M. & Scully R. Molecular analysis of sister chromatid recombination in mammalian cells. DNA Repair (Amst) 4, 149–61 (2005). [PubMed: 15590323]
69. Willis NA & Scully R. Measurement of Homologous Recombination at Stalled Mammalian Replication Forks. Methods Mol Biol 2153, 329–353 (2021). [PubMed: 32840790]
70. Willis NA, Panday A, Duffey EE & Scully R. Rad51 recruitment and exclusion of non-homologous end joining during homologous recombination at a Tus/Ter mammalian replication fork barrier. PLoS Genet 14, e1007486 (2018). [PubMed: 30024881]
71. Schmittgen TD & Livak KJ Analyzing real-time PCR data by the comparative C(T) method. Nat Protoc 3, 1101–8 (2008). [PubMed: 18546601]

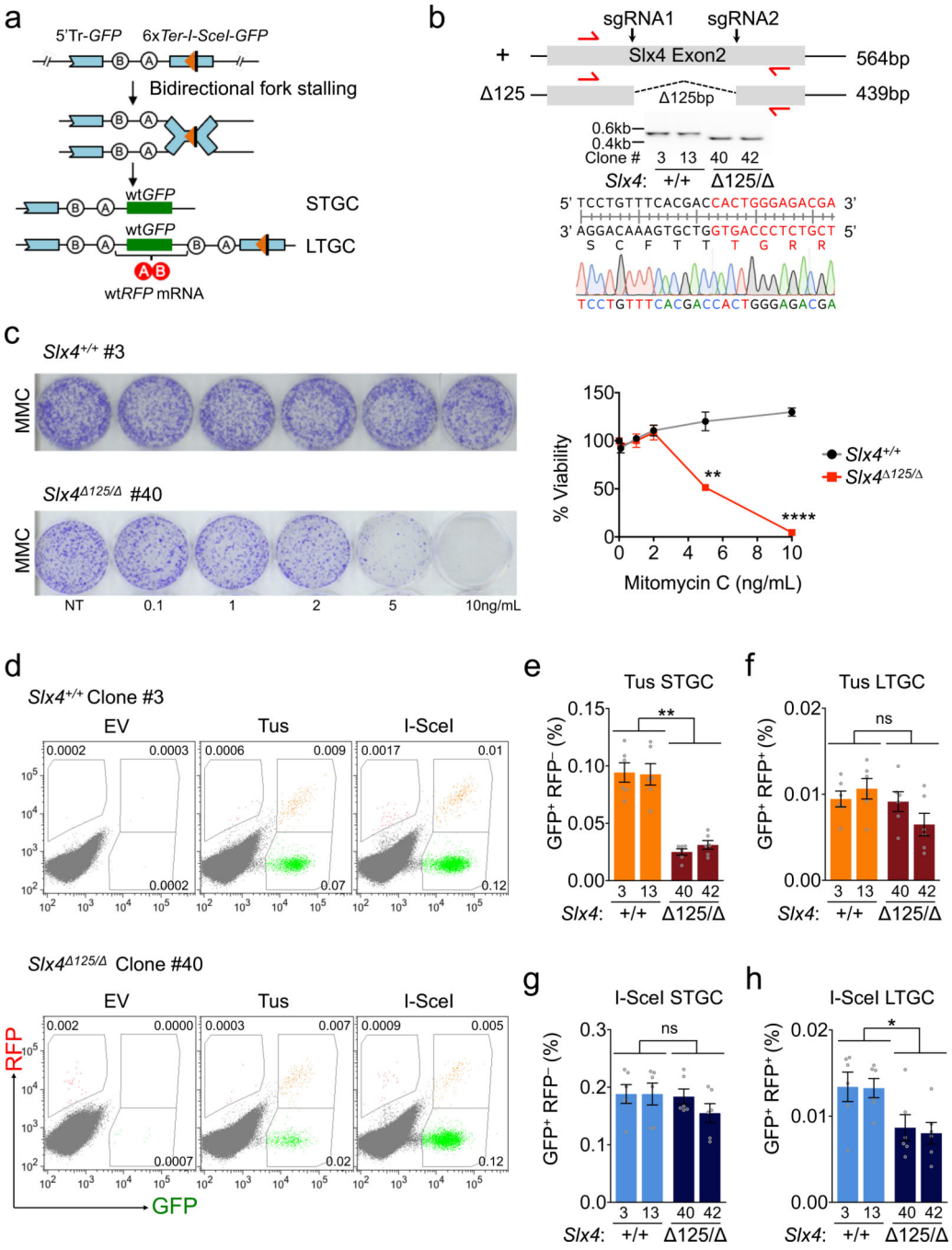

Fig. 1. *Slx4* regulates error-free HR at Tus/*Ter* stalled forks.

a. Schematic of 6x *Ter*-HR reporter and repair products of Tus/*Ter* induced fork stalling. Light blue boxes: mutant *GFP* alleles. Green box: wild type *GFP*. Open circles A and B: 5' and 3' artificial *RFP* exons, respectively. 5′ Tr-*GFP*: 5′-truncated *GFP*. Red triangle: 6x *Ter* array. Black line: I-SceI restriction site. STGC/LTGC, short/long tract gene conversion outcomes. LTGC generates wild-type *RFP* through RNA splicing (red filled circles). **b.** Strategy for generation of *Slx4*$^{\Delta 125}$ frameshift allele. Gel shows products of PCR of gDNA from *Slx4*$^{+/+}$ and *Slx4*$^{\Delta 125/\Delta}$ clones. Red letters above sequencing chromatogram indicate

frame shift. **c**. Representative images of colony formation assays performed in the presence of varying concentrations of Mitomycin C (MMC), in *Slx4*$^{+/+}$ (#3) (top) and one *Slx4*$^{\Delta 125/\Delta}$ (#40) (middle) cell lines. Right panel: Quantitation of above-mentioned colony formation assays, showing mean of three biologically independent replicates (n=3). Analysis using unpaired Student's *t*-test (n=3). P-value: **p < 0.01 and ****p < 0.0001. Error bars: s.d. **d**. Representative raw FACS data (uncorrected for transfection efficiency) for one *Slx4*$^{+/+}$ (#3) and one *Slx4*$^{\Delta 125/\Delta}$ (#40) 6x *Ter*-HR reporter clone co-transfected with either empty vector (EV), I-SceI or Tus expression vectors as shown. FACS plots produced from pooled technical duplicates, n=6. Numbers indicate percentages. **e** and **f.** Tus/*Ter*-induced STGC (**e**) and LTGC (**f**) in *Slx4*$^{+/+}$ clones and *Slx4*$^{\Delta 125/\Delta}$ clones. **g** and **h**. I-SceI-induced STGC (**g**) and LTGC (**h**) in *Slx4*$^{+/+}$ *vs*. *Slx4*$^{\Delta 125/\Delta}$ clones. Data in (**e-h**) shows mean values of n=6 biologically independent replicates. Error bars: standard error of the mean (s.e.m). Statistical analysis by ANOVA. In this and all subsequent figures: *p < 0.05; **p < 0.01; ***p < 0.001; ****p < 0.0001; ns, not significant.

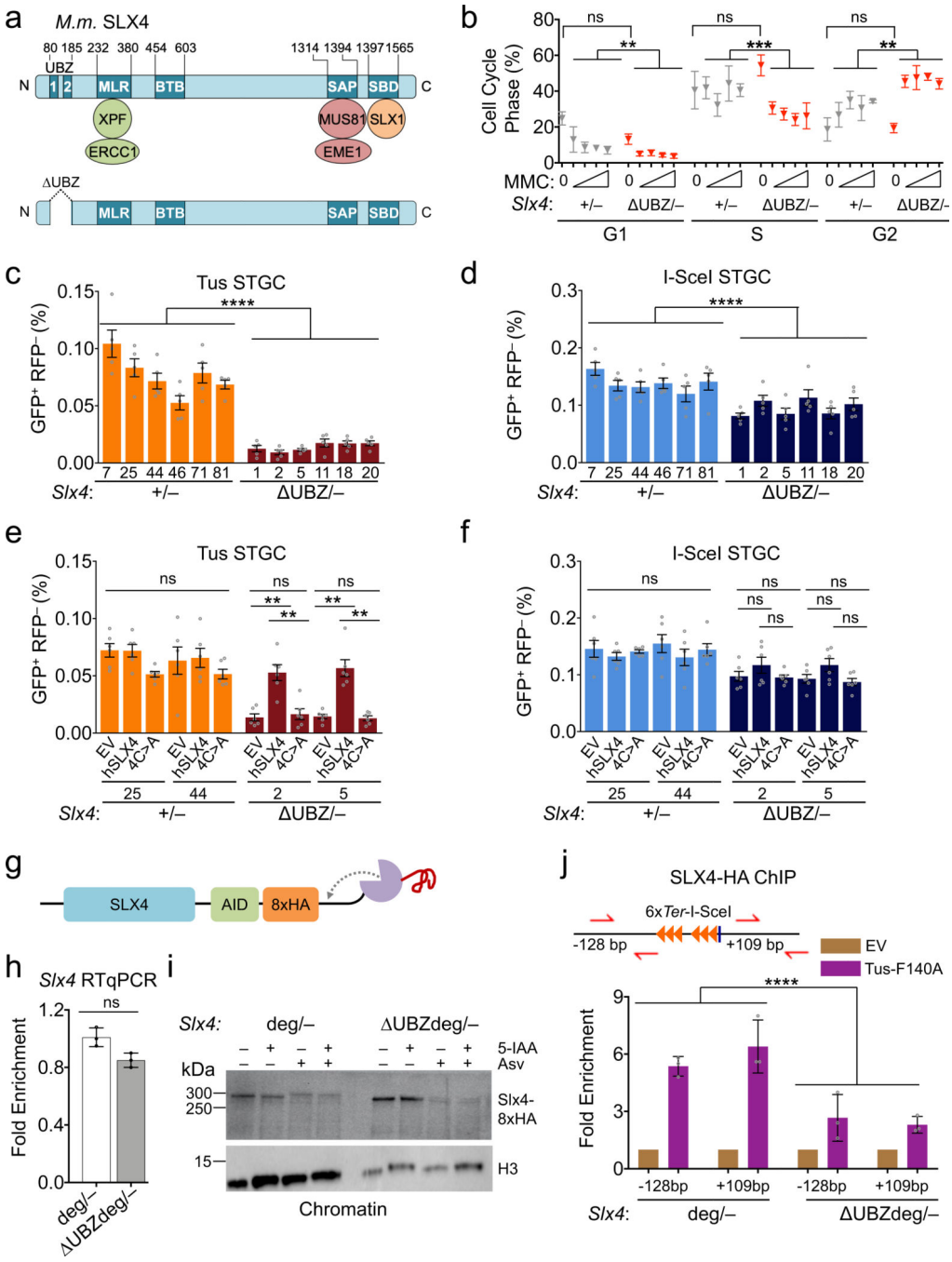

Fig. 2. The SLX4 UBZ domain mediates Tus/*Ter*-induced STGC by retaining SLX4 at stalled forks.

a. Schematic of SLX4 protein. MLR: XPF-interacting domain. SAP: MUS81-interacting domain. SBD: SLX1-interacting domain. Lower panel: SLX4 ΔUBZ protein. **b**. Cell cycle distribution of $Slx4^{+/-}$ and $Slx4^{\Delta UBZ/-}$ cells either untreated or treated with 20, 30, 40 or 50 ng/mL of MMC. Data shows mean values of three biologically independent replicates, n=3. Error bars: s.e.m. Untreated samples were compared using unpaired Student's *t*-test; MMC-treated groups were compared by one-way ANOVA. P-value: **p < 0.01; ***p <

0.001. **c** and **d**. Tus/*Ter*-induced STGC (**c**) and I-SceI induced STGC (**d**) in *Slx4*$^{+/-}$ *vs.* *Slx4*$^{\Delta UBZ/-}$ clones. Data shows mean values of five biologically independent replicates. Statistical analysis by ANOVA, n=5. P-value: ****p < 0.0001. Error bars: s.e.m. **e** and **f**. Impact of exogenous h*SLX4* on Tus/*Ter* induced STGC (**e**) and I-SceI induced STGC (**f**) in two independent *Slx4*$^{+/-}$ and two independent *Slx4*$^{\Delta UBZ/-}$ clones. EV: empty vector. 4C>A: h*SLX4* with inactivated UBZ motifs. Data shows mean values of six biologically independent replicates. Statistical analysis by unpaired Student's *t*-test, n=6. P-value: : **p < 0.01. Error bars: s.e.m. **g**. Schematic of *Slx4*$^{+/-}$and *Slx4*$^{\Delta UBZ/-}$ tagged with a dual degron containing a C-terminal 8xHA tag. **h**. RT-qPCR analysis of *Slx4* mRNA in *Slx4*$^{deg/-}$ and *Slx4*$^{\Delta UBZdeg/-}$ clones. Data normalized to *Gapdh* mRNA using the $2^{-\Delta CT}$ method. Expression of *Slx4*$^{\Delta UBZdeg/-}$ normalized to *Slx4*$^{deg/-}$. Each data point is an average of three technical replicates. Data shows mean of three independent biological replicates. Analysis by unpaired Student's *t*-test (n=3). Error bars: standard deviation (s.d.). **i**. Anti-HA immunoblot of HA-degron tagged SLX4, 24 hours after addition of degron-activating drugs 5-IAA and/or Asv. Asv: Asunaprevir. 5-IAA: 5-adamantyl-IAA. H3: Histone H3 loading control. **j**. Anti-HA ChIP analysis of SLX4-HA at Tus/*Ter* RFB in *Slx4*$^{deg/-}$ and *Slx4*$^{\Delta UBZdeg/-}$ cells. Each data point is an average of three technical replicates. Data shows mean of three independent biological replicates (n=3). Analysis by unpaired Student's *t*-test. P-value: ****p < 0.0001. Error bars: s.d.

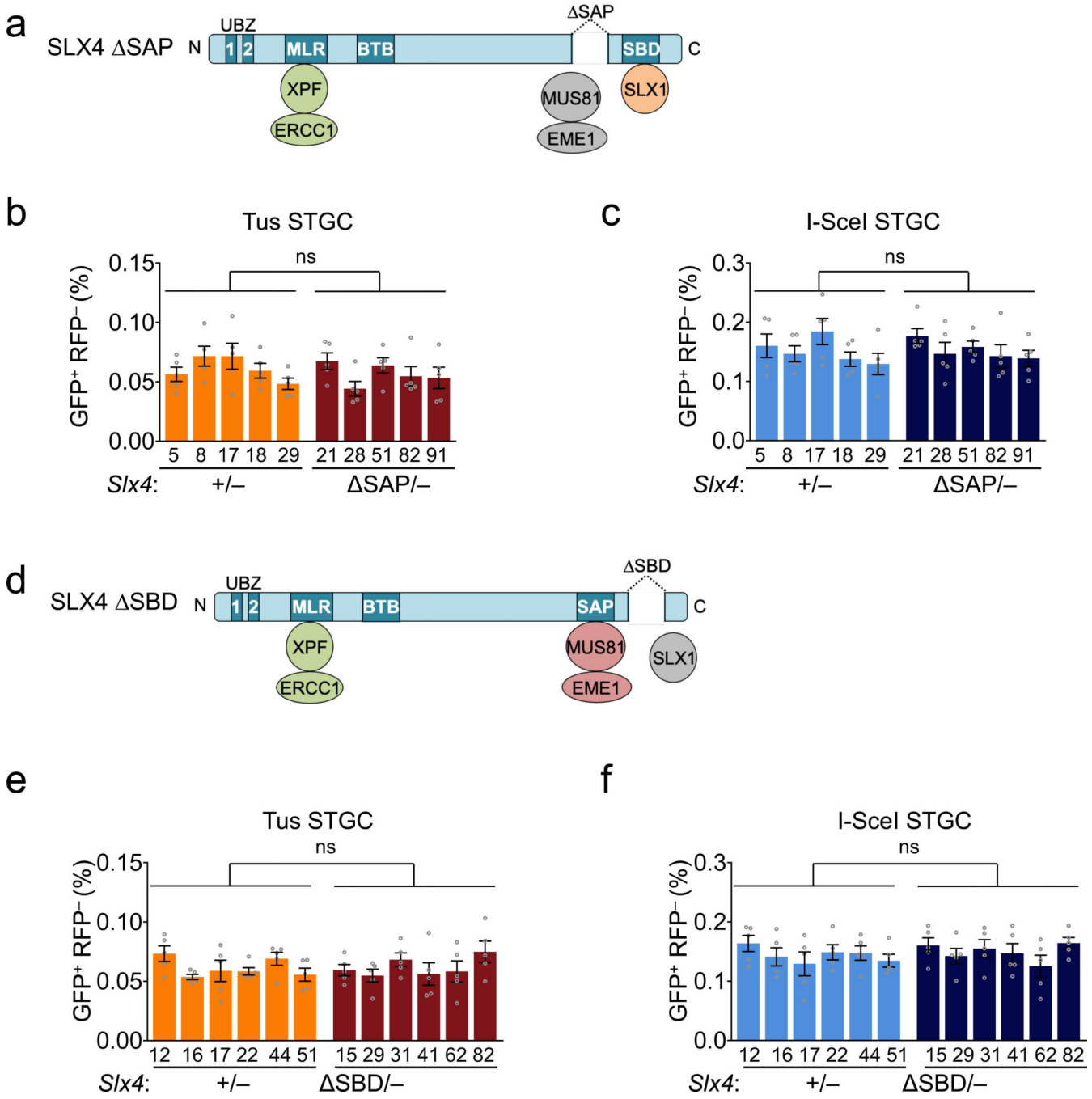

Fig. 3. Interactions of SLX4 with MUS81 and with SLX1 are dispensable for Tus/*Ter*-induced HR.

a. Schematic of SLX4 protein lacking the MUS81-interacting SAP domain. **b** and **c.** Tus/*Ter*-induced STGC (**b**) and I-SceI induced STGC (**c**) in *Slx4*$^{+/-}$ *vs.* *Slx4*$^{\Delta SAP/-}$ clones. Data shows mean values of five biologically independent replicates. Statistical analysis using ordinary one-way ANOVA, n=5. Error bars: s.e.m. **d**. Schematic of SLX4 protein lacking the SLX1-interacting SBD domain. **e** and **f.** Tus/*Ter*-induced STGC (**e**) and I-SceI induced STGC (**f**) in *Slx4*$^{+/-}$ *vs.* *Slx4*$^{\Delta SBD/-}$ clones. Data shows mean values of five biologically

independent replicates. Statistical analysis by ordinary one-way ANOVA, n=5. Error bars: s.e.m.

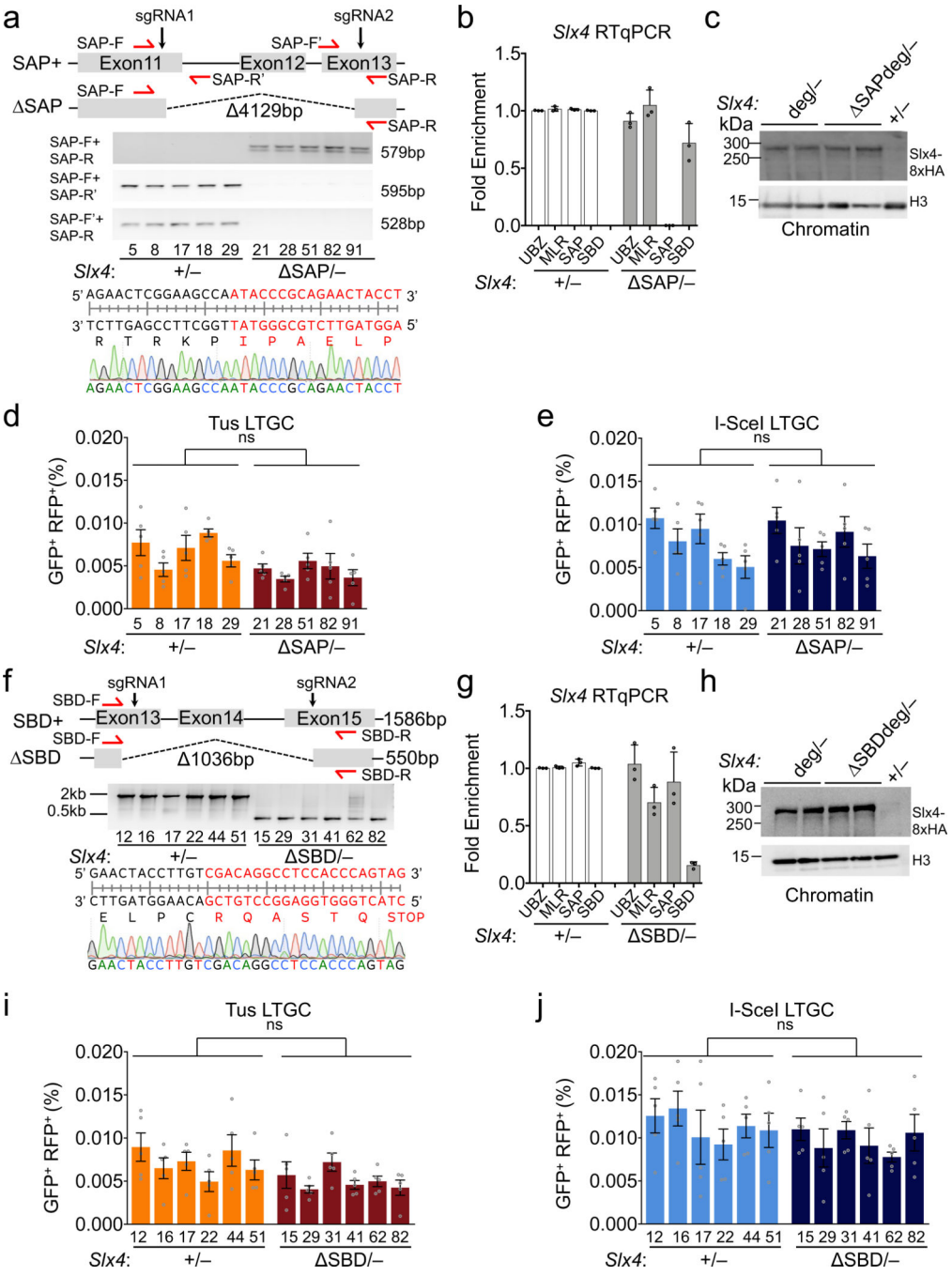

Fig. 4. Loss of the SLX4-XPF interaction causes a characteristic FA phenotype

a. Schematic of SLX4 protein lacking the XPF-interacting MLR domain. **b**. Cell cycle distribution of *Slx4*$^{+/-}$ and *Slx4*$^{\Delta MLR/-}$ cells either untreated or treated with 20, 30, 40 or 50 ng/mL of MMC. Data shows mean of three biologically independent replicates, n=3. Error bars: s.e.m. Untreated samples were compared using the unpaired Student's *t*-test; MMC-treated groups were compared by one-way ANOVA. P-value: *p < 0.05; ***p < 0.001; ****p < 0.0001. **c**. Representative images of metaphase spreads from *Slx4* mutants indicated, showing chromatid breaks (black arrows) and radial chromosomes (black

arrowheads) in untreated cells and cells treated with 20 ng/mL MMC for 12h **(d)** and **(e)**. Treated and untreated cells were harvested at the same time and each sample represented one independent experiment, n=1. Error bars: s.d. Quantitation of the number of breaks (**d**) and radial chromosomes (**e**) per metaphase nucleus in *Slx4*$^{+/-}$, *Slx4*$^{\Delta UBZ/-}$ and *Slx4*$^{\Delta MLR/-}$ cell lines. Analysis using unpaired Student's *t*-test. P-value: : *p < 0.05; **p < 0.01; ****p < 0.0001.

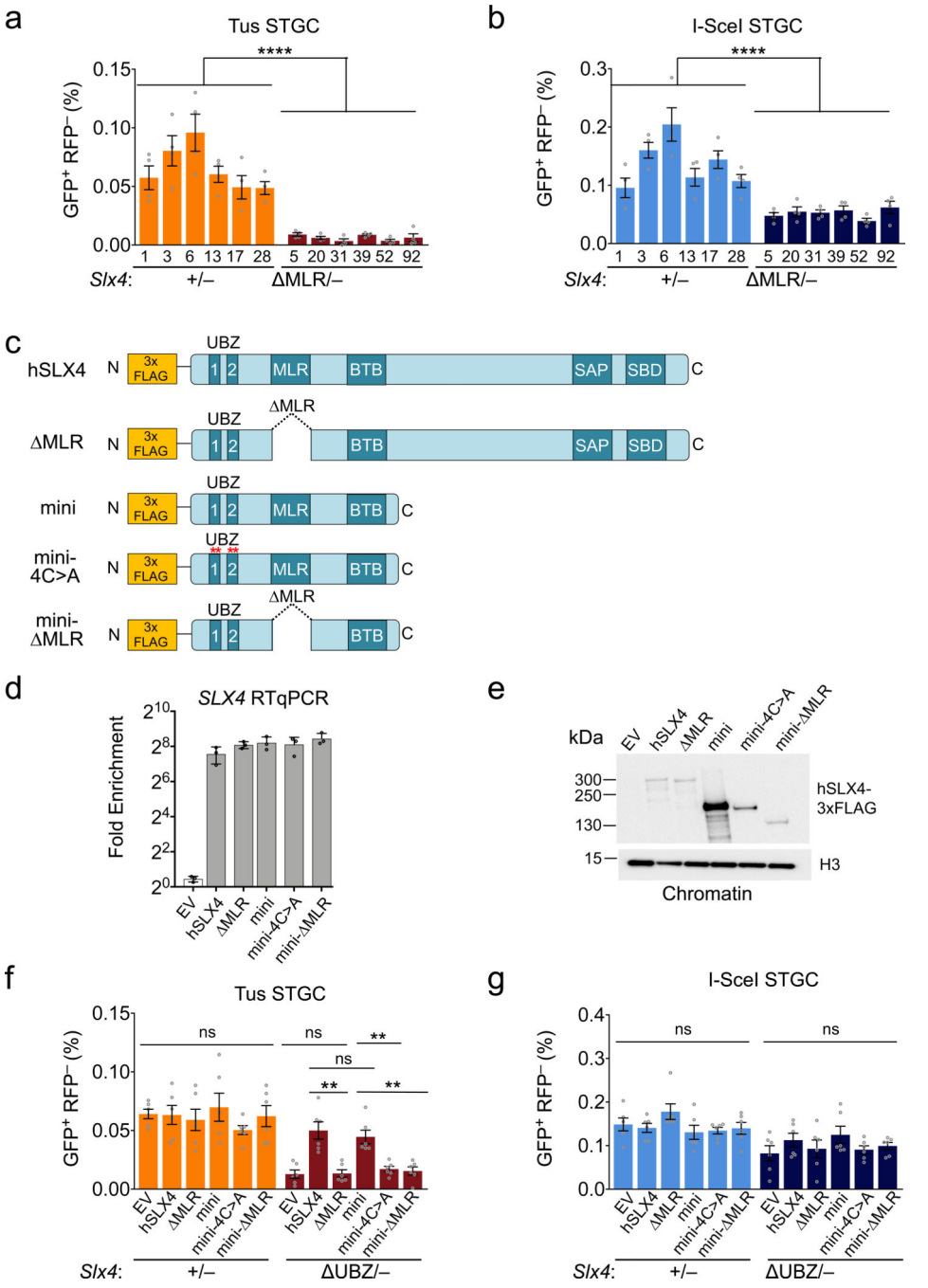

Fig. 5. The SLX4-XPF interaction is required for Tus/*Ter*-induced STGC.

a and **b** Tus/*Ter*-induced STGC (**a**) and I-SceI induced STGC (**b**) in $Slx4^{+/-}$ *vs.* $Slx4^{\Delta MLR/-}$ clones. Data shows mean values of five biologically independent replicates, n=4. Analysis by one-way ANOVA, P-value; ****p < 0.0001. Error bars: s.e.m. **c.** Schematic showing mutants of human *SLX4* used for transient expression experiments. **d**. RT-qPCR analysis of expression of human *SLX4* variants in mES cells. *SLX4* expression normalized to *Gapdh* and displayed as fold difference compared to empty vector (EV) of the same experiment. Each data point is an average of three technical replicates. Data shows mean of three

independent biological replicates, n=3, Error bars: s.d. **e**. Western blot analysis of the chromatin-bound fraction of various human 3xFLAG-SLX4 mutants transiently expressed for 48 hours and blotted with anti-FLAG antibody. **f** and **g**. Impact of h*SLX4* variants on Tus/*Ter*-induced STGC (**f**) and I-SceI-induced STGC (**g**), following transient *SLX4* expression in *Slx4*$^{+/-}$ and *Slx4*$^{\Delta UBZ/-}$ *Ter*-HR reporter clones. Analysis was performed using unpaired Student's *t*-test, n=6. Error bars: s.e.m. P-value: **p < 0.01.

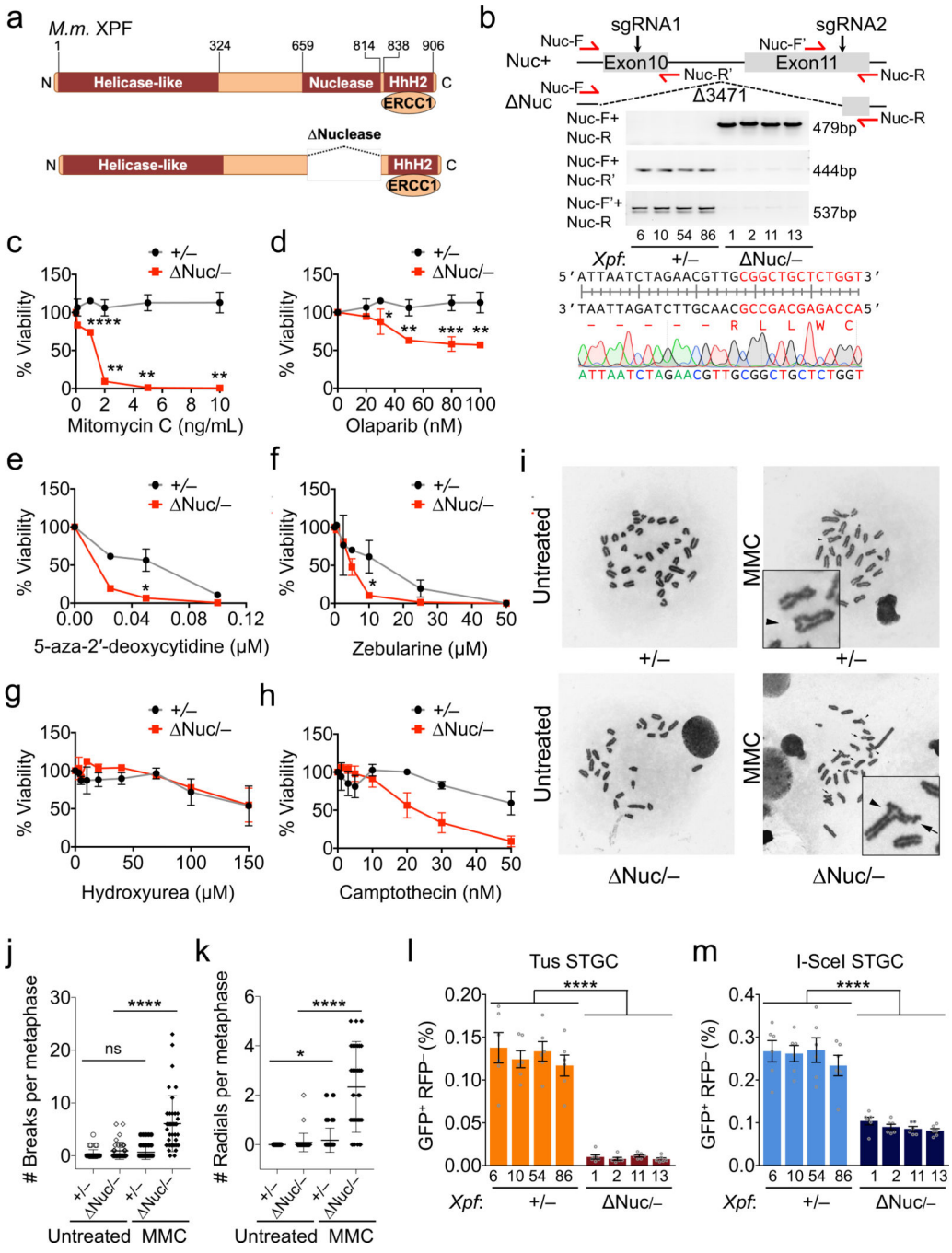

Fig. 6. The XPF nuclease domain is required for Tus/*Ter*-induced STGC.

a. Schematic of wild type XPF protein and XPF mutant lacking the nuclease domain. **b**. Strategy for generating $Xpf^{\Delta Nuc}$ allele. Red half-arrow heads: genotyping primers. Gel shows PCR products on gDNA from $Xpf^{+/-}$ and $Xpf^{\Delta Nuc/-}$ clones and sequencing chromatogram showing the breakpoints in the in-frame mutant (#6) **c**-**h**. Quantification of colony formation of $Xpf^{+/-}$ *vs.* $Xpf^{\Delta Nuc/-}$ clones in the presence of MMC (**c**) or Olaparib (**d**) 5-aza-2′-deoxycytidine (**e**) Zebularine (**f**) Hydroxyurea (**g**) and Camptothecin (**h**). Data show mean of three biologically independent replicates normalized to untreated samples

(n=3). Analysis using unpaired Student's *t*-test. P-value: *p < 0.05; **p < 0.01; ***p < 0.001; ****p < 0.0001. Error bars: s.d. **i**. Representative images of metaphase spreads showing chromatid breaks (black arrows) and radial chromosomes (black arrowheads) from indicated *Xpf* mutant cells, either untreated or treated with 20 ng/mL MMC for 12h. **j** and **k**. Quantitation of the number of chromatid breaks (**j**) radial chromosomes (**k**) per metaphase in $Xpf^{+/-}$ (#6) and $Xpf^{\Delta Nuc/-}$(#1) clones. Treated and untreated cells were harvested at the same time and each sample represented one independent experiment, n=1, Analysis using unpaired Student's *t*-test. P-value: *p < 0.05; ****p < 0.0001. Error bars: s.d. **l** and **m**. Tus/*Ter*-induced STGC (**l**) and I-SceI induced STGC (**m**) in $Xpf^{+/-}$ *vs.* $Xpf^{\Delta Nuc/-}$ clones. Data shows mean values of six biologically independent replicates, n=6. Analysis by one-way ANOVA. P-value: ****p < 0.0001. Error bars: s.e.m.

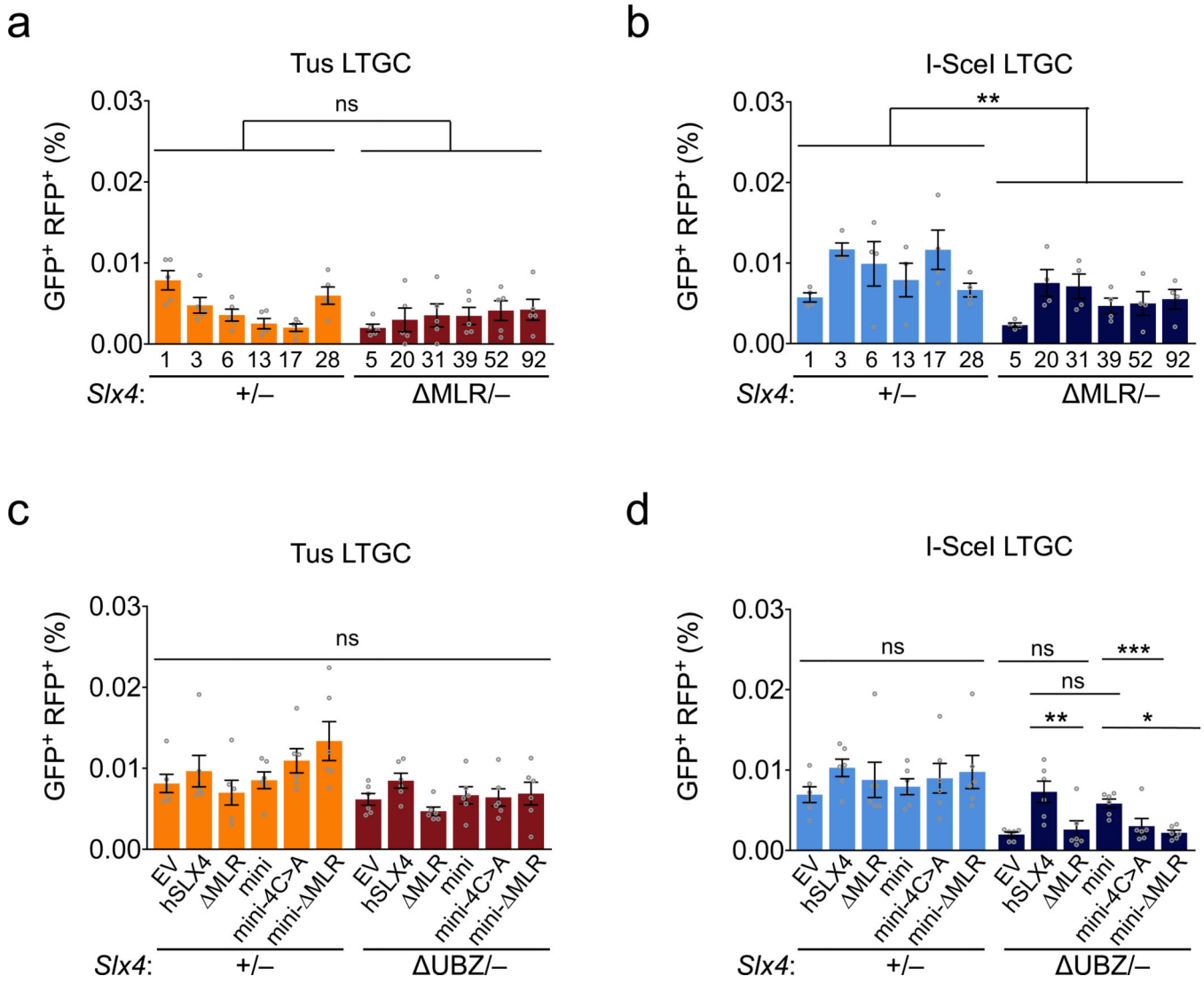

Fig. 7. Model of SLX4 action in Tus/*Ter*-induced HR.

a. In wild type cells, FA pathway activation and asymmetric fork reversal at forks bidirectionally stalled at Tus/*Ter* RFB enables SLX4 recruitment and its retention at the stall site, mediated by interactions of the SLX4 UBZ domain with as yet unidentified ubiquitinated components at the stall site. SLX4 MLR domain enables recruitment of XPF-ERCC1, which incises the stalled leading strand of at least one sister chromatid (incision *a*, red triangle). Note that the second incision (red triangle *b*), which would be required for ICL unhooking, may be redundant for generation of a DSB at Tus/*Ter*, since there is no ICL. The two-ended DSB generated by SLX4-XPF is repaired by conservative HR (STGC). **b.** In cells lacking the SLX4 UBZ domain, retention of SLX4-XPF at the stall site is impaired, leading to inefficient incision of the stalled forks and reduced DSB formation. There is a corresponding defect in Tus/*Ter*-induced STGC. **c.** In cells lacking the SLX4 MLR domain, or lacking the XPF nuclease domain, XPF-mediated incision of the stalled forks is abolished, resulting in a severe defect in Tus/*Ter*-induced STGC.